POLITEKNIK NEGERI BALI

Journal of Engineering Design and Technology

logic

Vol. 19 No. 1 March 2019

LOGIC

Jurnal Rancang Bangun dan Teknologi

p-ISSN. 1412-114X

e-ISSN. 2580-5649

LOGIC

Jurnal Rancang Bangun dan Teknologi

Journal of Engineering Design and Technology

Gedung P3M, lt.1 Politeknik Negeri Bali, Bukit Jimbaran
PO BOX 1064 Kuta Selatan, Badung, Bali - Indonesia
Telp. (+62)361 701981 Fax. (+62)361 701128
Email: logic@pnb.ac.id

LOGIC JOURNAL TEAM

PREFACE

Logic: Jurnal Rancang Bangun dan Teknologi (Journal of Engineering Design and Technology) is a peer-reviewed research journal aiming at promoting and publishing original high quality research in all disciplines of engineering and applied technology. All research articles submitted to Logic should be original in nature, never previously published in any journal or presented in a conference or undergoing such process across the world. All the submissions will be peer-reviewed by the panel of experts associated with particular field. Submitted papers should meet the internationally accepted criteria and manuscripts should follow the style of the journal for the purpose of both reviewing and editing.

Logic is a journal covering articles in the field of civil and mechanical engineering, design, and technology published 3 times a year in March, July, and November. Language used in this journal is English.

LOGIC. P-ISSN 1412-114X
LOGIC. E-ISSN 2580-5649
Indexing : GOOGLE SCHOLAR, DOAJ, EBSCO OPEN SCIENCE DIRECTORY, SINTA 4

Best Regard,

LOGIC Editorial Team

TABLE OF CONTENTS

LOGIC
Journal of Engineering Design and Technology
Vol. 19 No.1 March 2019; p. 1 - 6

p-ISSN : 1412-114X
e-ISSN : 2580-5649
http://ojs.pnb.ac.id/index.php/LOGIC

ERROR OPTIMIZATION IN ELECTRICAL POWER QUALITY MONITORING DATA

[1,2,3)] Electrical Engineering Department, Politeknik Negeri Jakarta, Depok, Indonesia

Correponding email [1)] : isdawimah@elektro.pnj.ac.id

Isdawimah[1)], Ismujianto[2)], A.Damar Aji[3)], Nuha Nadhiroh[4)]

Abstract.In the application of electrical power quality control, the necessity for data processing becomes very important. The measurement data obtained is the latest data and measured in real time with good time resolution and with low error. The object of research is the quality of electric power, the research is about ways of measuring quality of electrical power to obtain accurate data in accordance with actual conditions. This method is capable of measuring data of electrical power quality that changes very quickly with a low error. This data is used as a basis for improving the quality of electric power accurately and accurately.

Keywords :Data Measurement, Error, Power Quality, Monitoring, Signal Sampling

1. INTRODUCTION

The high level of harmonic distortion in the electrical power distribution system can result in overheating of the equipment and the conductors, permanent damage for some sensitive electronic equipment, reduced equipment lifetime and cause reading errors up to 17.2% on kWh meters [1]. Apart from the load used by consumers, harmonics can also come from utilities (electrical resources) themselves.Several methods for identifying harmonic sources have been found, such asharmonic identification methods based on Thevenin Theorem, active power method, Norton Theorem method, time-reactive power gradient method, and harmonic and interharmonic estimation methods [2].

Another reason for the decrement in electrical power quality is the occurrence of voltage dip or a momentary voltage interruption. The occurrence of voltagedip for 0.5-3 seconds [3] or more can cause the computer to shut down, loss of data memory, loss of motor as load, trip conditions on variable speed drives, causing disruption to industrial machine operations and losses due to failure of the production process [4]. Flicker in the European standard EN 50160 is defined as a visible change in brightness of a lamp due to rapid fluctuations in the voltage of the power supply.

Provision of good and constant quality electricity can be done by controlling the following parameter: voltage, current, frequency, phase angle, power and harmonic order. Controlling electrical power quality can be done if the value of the existing electrical parameter is measureable continuously and compared with the standard value. While the data value change is fast and the latest data is strongly required, it is necessary to carry out continuous monitoring with a good data acquisition system.

Monitoring the quality of electric power using conventional measuring devices can only obtain limited data [5]. Monitoring the quality of electric power is used as the basis for reconfiguring neural networks in the three-phase system [6]. In the monitoring system must pay attention to good time and frequency resolution, in order to obtain optimal electrical power quality monitoring data [7]. Monitoring is used in the smart grid system to inform in real time about the use of electrical energy and costs to be paid by users [8]. Voltage monitoring using a Neural Network on a distribution system in a remote area is carried out using only signals from the utility substation [9].

In controlling electrical power quality system, the necessity for data collection and processing becomes

very important.The obtained measurement data must be up-to-date and measured in real time with good time resolution and low error. The measured data is in the current and voltage waveform with varying forms and with very rapid changes in value due to various disturbances, such as harmonics, voltage dip, flicker and so on.Therefore, a particular method is needed so that these waveform changes can be read and measured completely in accordance with the actual conditions (low error). Real time data will serve as a basis for improving the quality of electrical energy sources.

Numerical methods are used to formulate mathematical problems, so that they can be solved by arithmetic operations. The result is a value that the approximation of actual value with a level of accuracy as desired.In this case there will be an error because the resulting value is not exactly the same as the actual value.One type of error is a truncation error that is related to the number of sampling that is limited to a certain term (n-*th*).Truncation error occurs because it doesn't use all the values in the series, where the number of rows is infinite. This omitted values produces a cutting error.

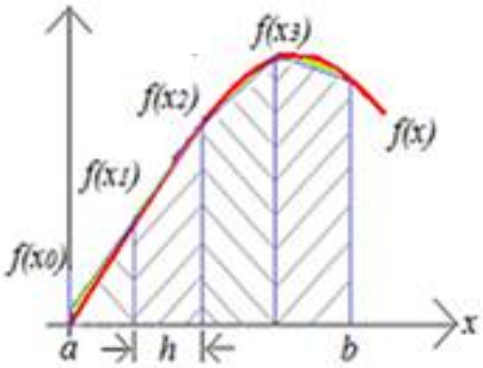

Figure 1. Signal Sampling in Trapezoid

The signal sampling method used in this research is the trapezoidal method, where the signal is copied into the form of a trapezoid with a certain amount of sampling as shown in Figure 1. The trapezoidal method generates series as follows:

$$Y = \frac{(b-a)}{2n}[f(x_0) + 2\sum_{i=1}^{n-1} f(x_i) + f(x_n)] \quad (1)$$

Where:

$$\bar{f}^{(2)} = \frac{\int_a^b f^{(2)} dx}{(b-a)} \quad (2)$$

With the amount of singnal sampling as:

$$n = \sqrt{\left[\frac{(b-a)^3}{12\varepsilon}\bar{f}^{(2)}\right]} \quad (3)$$

And the error will be:

$$\varepsilon_n = \frac{(b-a)^3}{12n^2}\bar{f}^{(2)} \quad (4)$$

2. METHODS

The monitoring system consists of data retrieval programs using LabVIEW software, voltage and current sensors, analog to digital signal converter circuits (ADC), while a personal computer (PC) are being used for displaying the data.The objectivesof the monitoring system are collectingmeasurement data, converting data from analogue into digital signals, displaying and storing data on a PC. Measurement data is processed by LabVIEW software and displayed in real time. Then, the data are sent to the control system. Data processing based on EN50160 standard. While the classification of electrical power quality disturbances is based on the IEEE Power and Energy Society.

The flow of converting analogue to digital signals through several procedures: sampling, quantization and coding. The focus of this research is on the signal sampling process that is related to the selection of the signal sampling method so that the minimum number of sampling is possible with the lowest possible error. The number of signal samplings is very important in order to make an efficient number of bytes needed in ADC process. In this case the smallest number of signal clicks is selected. The algorithm for determining the number of signal

flashes in the ADC process is shown in Figure 2. Firstly, the process of determining the number of signal flashes is done by knowing the series function of a waveform (current or voltage) called f(x). Secondly is determining the waveformoperational area that already limited by the magnitude a and b.

As describe above, the measured waveform is close to the sinusoidal shape, therefore this research only uses trapezoidal form for signal sampling method. To determine the number of signal samplings in trapezoidal form (n_1) we need a second derivative of f(x), called $f^{(2)}$ which is calculated using equation (2), while n_1 and n_2 are calculated using equation (3). Then the result of n_1 and n_2 are compared and selected based on the smallest number of signal samplings.

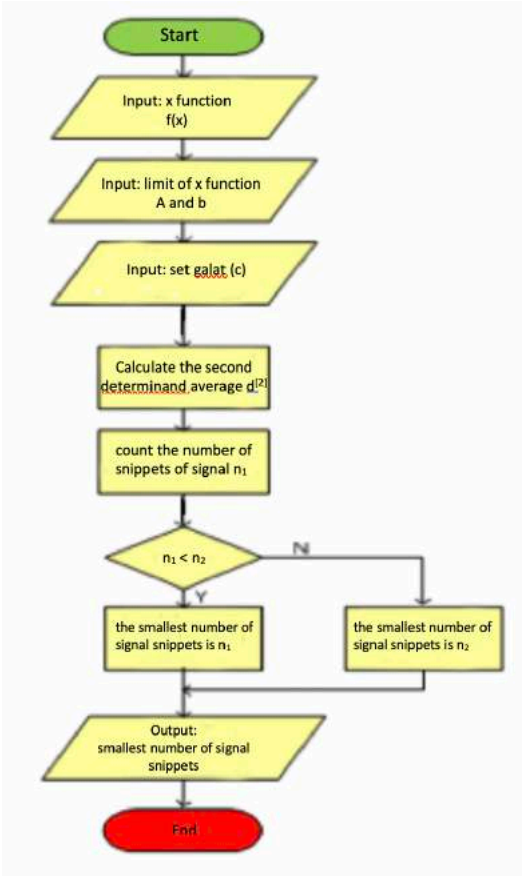

Figure 2. The Algorithm of Optimization Signal Samplings

3. RESULTS AND DISCUSSION

The voltage equation consists of a voltage at fundamental frequency and a voltage at a ripple frequency:

$$V_{inv} = V + V_k$$

$$V_{inv} = V_m \sin\theta + V_{mk} \sin k\theta \quad (5)$$

If the voltage in equation (5) is copied n-times with the trapezoidal shape at the boundaries a = 0 and b =, then the voltage equation is obtained as below:

$$V_{inv} = \frac{\pi}{2n}\left[(V_m \sin\theta_0 + V_{mk} sin\ k\theta_0) + 2\sum_{i=1}^{n-1}(V_m \sin\theta_i + V_{mk} sin\ k\theta_i) + (V_m \sin\theta_n + V_{mk} sin\ k\theta_n)\right] \quad (6)$$

the second derivative f(x) with k-odd numbers is:

$$\bar{f}^{(2)}(V_{inv}) = \frac{-2}{\pi}[V_m + kV_{mk}] \quad (7)$$

After obtaining the average of second derivative, the voltage signal sampling error can be calculated based on equation (4):

$$\varepsilon_V = \frac{-\pi^2}{6n^2}[V_m + kV_{mk}] \quad (8)$$

And the number of signal samplings (n) for a particular error value is:

$$n = \left[\frac{\pi^2}{6|\,\varepsilon_V|}[V_m + kV_{mk}]\right]^{1/2} \quad (9)$$

After obtaining the number of signal samples based on equation 9, a graph of the relationship between the number of sampling signals is made with the measured voltage (Figure 5).In addition, errors also occur as a result of sampling signals using equation 8 and graphically as illustrated in Figure 6.Data was taken on MDP power panels for five classes of the Electric Laboratory and four classes of the Politeknik Negeri Jakarta Electrical Workshop (Figure 3). The waveform as the results of signal samplings is shown in Figure 4, where the waveform will approach the actual shape if the number of samples is very large.

The measured voltage is less than the reference voltage when sampled with an amount of less than 80.The value of this voltage increases as the number of signals increases (Figure 5). This affects the error that occurs with an average voltage error of (-0.02843), where the error decreases as the number of signals increases (Figure 6).

Figure 3. Electrical power quality measurement location

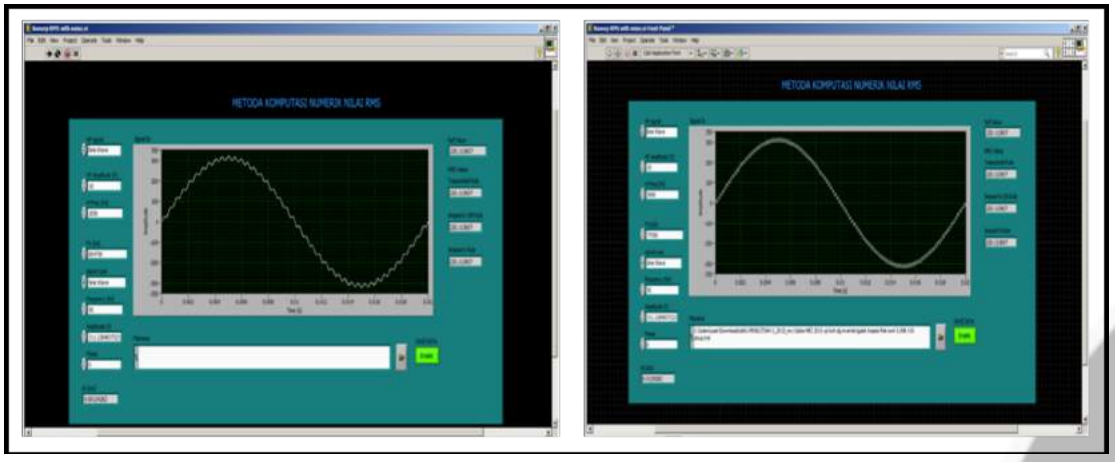

Figure 4. Signal Sampling for Sinusoidal

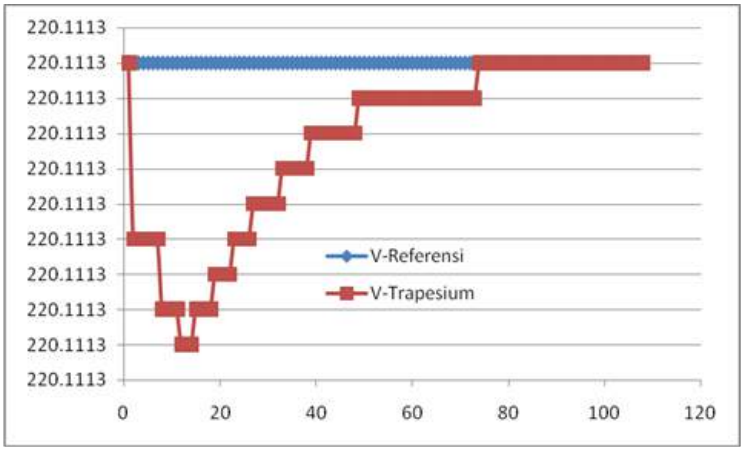

Figure 5. Number of signal samplings for measured voltage

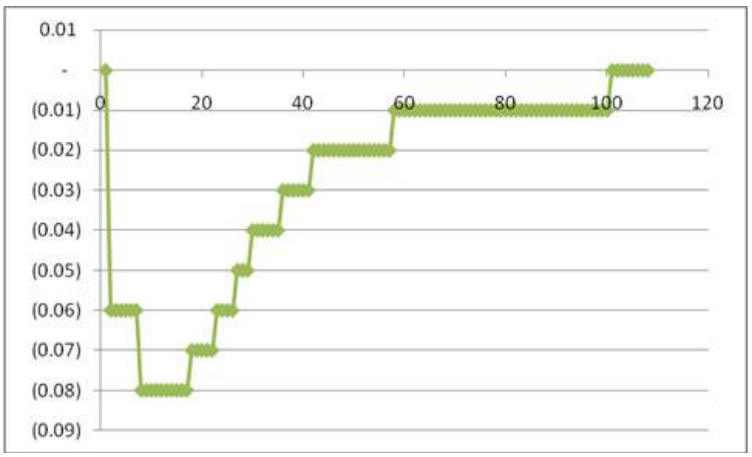

Figure 6. Graphic of error as a result of signal samplings

4. CONCLUSION

Based of result and discussion above, the conclusions of this research are:

a. The voltage equation consists of voltage at the fundamental frequency and voltage at the ripple frequency. If the voltage is taken as many times as the trapezoidal shape, an error will occur
b. The measured voltage is less than the reference voltage when sampled with an amount of less than 80. The value of this voltage increases as the number of signals increases
c. The amount of signal sampling affects the error that occurs with an average voltage error of (-0.02843), where the error decreases as the number of signals increases

5. REFERENCES

[1] Isdawimah, R. Setiabudy, and R. Gunawan (2014). The Effect of High Switching Frequency on Inverter Against Measurements of kWh-Meter. *IPTEK Journal of Proceedings Series*, vol. 1, pp. 102-108.
[2] I. Sadinezhad and V. G. Agelidis (2011). Slow Sampling on-line Harmonics/interharmonics Estimation Technique for Smart Meters. *Electric Power Systems Research 81 Elsevier Journal*, pp. 1643-1653.
[3] IEEE Power and Energy Society (2015). Electrical Signatures of Power System Failures. *IEEE The Institute of Electrical and Electronic Engineers*, Inc
[4] F. Salim, K. M. Nor, D. M. Said (2012). Experience in Online Power Quality Monitoring Through VPN. *International Conference High Quality of Power (ICHQP) 15th*, IEEE
[4] Soner Emec, Jörg Krüger, Günther Seliger (2016). Online fault-monitoring in machine tools based on energy consumption analysis and non-invasive data acquisition for improved resource-efficiency. *13th Global*

Conference on Sustainable Manufacturing - Decoupling Growth from Resource Use, www.elsevier.com/locate/procedia

[6] Martin Valtierra-Rodriguez et al. (2013). Reconfigurable instrument for neural-network based power-quality monitoring in 3-phase power systems. *IET Journal Generator Transmission Distribution*, 7, Iss. 12, pp. 1498–1507

[7] Mahdi Hajian, Asghar Akbari Foroud, Ali Akbar Abdoos (2013). New automated power quality recognition system for online/offline monitoring. *Neuro computing Journal*, 128, 389–406 journal homepage: www.elsevier.com/locate/neucom

[8] Bochu Subhash and V.Rajagopal (2014). Overview of Smart Metering System in Smart Grid Scenario. *Power and Energy Systems: Towards Sustainable Energy (PESTSE 2014)*

[9] Alex S. Silva, Ricardo C. dos Santosa, Fernando B. Bottura, Mário Oleskovicz (2017). Development and evaluation of a prototype for remote voltage monitoring based on artificial neural networks. *Engineering Applications of Artificial Intelligence Journal*, 57, 50–60. journal homepage: www.elsevier.com/locate/engappai

LOGIC
Journal of Engineering Design and Technology
Vol. 19 No. 1 March 2019 ; p. 7 - 13

p-ISSN : 1412-114X
e-ISSN : 2580-5649
http://ojs.pnb.ac.id/index.php/LOGIC

REDESIGN OF CLOVE DRYER SIMULATION MACHINE USING HEAT WASTE OF RADIATOR AS THE HEAT SOURCE

I Kadek Ervan Hadi Wiryanta [1)], I Gusti Agung Mas krisna Komala Sari [2)], I Made Anom Adiaksa [3)]

1) Mechanical Engineering Department, Bali State Polytechnic, Kampus Bukit Jimbaran Street, Badung, Bali, Indonesia
2) Tourism Department, Bali State Polytechnic, Kampus Bukit Jimbaran Street, Badung, Bali, Indonesia
3) Mechanical Engineering Department, Bali State Polytechnic, Kampus Bukit Jimbaran Street, Badung, Bali, Indonesia

Correponding email [1)] : ervanhw@pnb.ac.id

Abstract. In this study, a redesign to a clove dryer simulation tool using exhaust heat from radiator as a source of heat energy has been done. The dryer simulation tool consists of reservoir tank, a heater, a pump to circulate the water in the system, a radiator as a heat exchanger and a drying chamber with 2 shelves. The redesign stage is carried out by fixing the piping insulation system, changing the pipe and adding valve controls to vary the velocity of the fluid flow. Variations made are variations in the mass flow rate of 0.09 kg / s and 0.18 kg /s with a constant air flow rate of 1 m/s. The results of the analysis show that at a higher mass flow rate of 0.18 kg/s the average rate of heat transfer from the radiator air side is higher, which is around 3971.65 watts. The effectiveness of the radiator will also be higher at a higher mass flow rate, the average is 0.34 at a mass flow rate of 0.09 kg/s and 0.43 at a mass flow rate of 0.18 kg /s. For drying rates with a load of 2 kg of cloves with a higher flow rate of liquid will be faster, which is about 5 hours with a flow rate of 0.18 kg/s and 6.5 hours at a flow rate of 0.09 kg/s

Keywords : Redesign, Dryer Simulation, Radiator Heat Waste, Fluid Flow Variation.

1. INTRODUCTION

Radiator is a compact heat exchanger that is used to transfer heat energy from one medium to another for the purpose of cooling and heating. As a compact heat exchanger, the radiator has various types depends on the configuration of the radiator core. So far, radiators are widely known in the automotive industries as a tool to control the temperature of the engine so that the engine temperature stays in the optimal condition between 80°C - 90°C. As a heat exchanger, the radiator certainly produces a waste product in the form of exhaust heat which of course can be used for heating or drying purposes.

For a drying purpose, it is important to know the performance of the radiator first, especially those related to the results of the exhaust heat that can be produced by the radiator. Several studies of radiator performance have been carried experimentally and numerically by varying the mass flow rate of fluid flow in the radiator. This is done in several conditions and by using several different working fluids. An experimental research has been analyzed in a corrugated plate type heat exchanger, where the result showed that the heat transfer coefficient increases with the increasing of mass flow rate for various working fluids. [1]. The experiment to knows the effect of the heat transfer characteristic in automotive radiator has been done by varying the coolant flow rate, with the result showed that the increasing of coolant flow rate will also increasing the Nusselt (Nu) number of the coolant. [2]. Experiment to analyze the effect of mass flow rate on the convective heat transfer coefficient also done to a constant velocity on constant area. [3]. An experimental was also carried out to determine the effect of mass flow rate on pressure drop and heat transfer in a drying chamber, which the result showed that the higher the temperature at the drying chamber inlet, the lower the pressure drop. The pressure drop will increase with the increasing of mass flow rate. [4]. Numerical research has also done to analyze mass flow rate effect to the heat transfer rate of automobile radiator using CFD

modeling, and the result showed that as the air mass flow rate increases, the heat transfer rate as well as efficiency is also increasing. [5].

Based on the description, in this research will be carried out a simple redesign of existing drying equipment by changing several components of the previous system that have been carried out, such as variations in fluid flow velocity. The performance observed are the effectiveness and also the air-side temperature and heat transfer rate of the radiator, so that it will get a good drying result in the drying chamber.

2. METHODS

The research was carried out experimentally by redesigning the system in the simulation of the previous dryer that made by [6]. The redesign is done by varying the speed of fluid flow inlet the radiator system by using a valve and flowmeter, so that the radiator can get optimal heat dissipation performance. The other components in previous dryer tools such as used tube and fins type radiators, water reservoir tanks, heaters, hot water pumps, thermostat, and cooling fans are still used by checking and repairing several components that have been broken, such as the thermostat, and replaced piping insulation system to get more effectiveness in radiator performance. The schematic of the system are shown in figure. 1 below

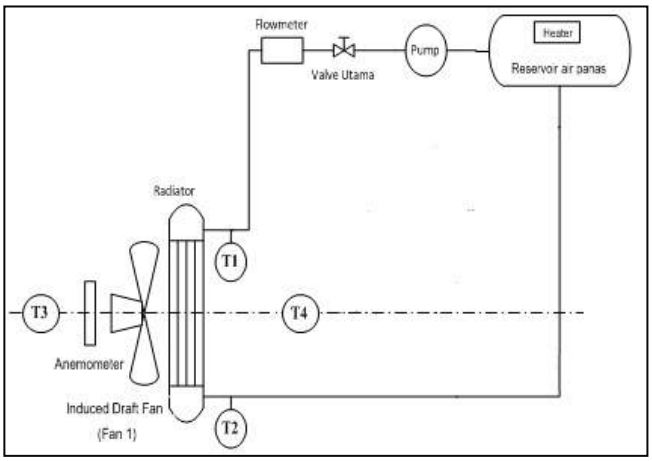

Figure 1 Schematic experimental set-up

The radiator's specification used in this research showed in table 1 below

Table 1 Specification of Radiator

No	Data	Values
1.	Radiator's type	*Compact heat exchanger- circular tube continuous fin*
2.	Radiator's volume	P x L x T= 500mm x 30 mm x 550 mm
3.	Tube diameter	10 mm
4.	Tube length	330 mm
5.	Number of row	2
6.	Number of tube per row	22
7.	Pitch	11 mm

Analysis of radiator performance is done by using the equation for compact heat exchanger analysis as in the following equation [7], [8] there were:

Coefficient convection (hcold) :

$$h_{cold} = St.\ G.\ Cp \quad (1)$$

Heat transfer rate (qcold) :

$$q_{cold} = h_{cold}.A_{cold}\ (\ Tc_{in} - Tc_{out}\ ) \quad (2)$$

Effectiveness radiator (ε) :

$$\varepsilon = \frac{q_c}{q_{max}} = \frac{Ch\ (Thi\text{-}Tho)}{Tmin\ (Thi\text{-}\ Tci)} = \frac{Cc\ (Tco\text{-}Tci)}{Cmin\ (Thi\text{-}Tci)} \quad (3)$$

where :

$q_{max} = Cmin \,.\, (Th,_i - Tc,_i)$ (4)

$Ccold = \dot{m}_c \,.\, Cp_c$ and $Ch = \dot{m}_h \,.\, Cp_h$ (5)

3. RESULTS AND DISCUSSION

3.1 Redesigning Clove Dryer

Before redesigning the dryer, an analysis is first carried out to calculate the inlet radiator water flow rate to produce the most effective heat exhaust for clove drying. According to [9], the drying room temperature is 40-60 ˚C with an average of 52.02 ˚C for drying cloves. From the data, the initial calculation is done to determine the velocity of the fluid flow inlet the radiator using the effectiveness radiator's analysis from equation above.

T = 40°-60°
Average Temperature = 52,02° C
Assuming :
T1 = 70° C -> 343 K
T2 = 50° C -> 323 K
T3 = 30° C -> 303 K
T4 = 42° C -> 315 K
Radiator's effectiveness

$$\varepsilon = \frac{Tco - Tci}{Thi - Tci} => \frac{T4 - T3}{T1 - T3}$$

$$\varepsilon = \frac{315-303}{343-303} = \frac{12}{40} = 0,3$$

$$\varepsilon = \frac{q}{q_{max}} = \frac{\dot{m}c \,.\, Cc \,.\, (Tco - Tci)}{\dot{m}h \,.\, Ch \,(Thi - Tci)}$$

Air flow rate ($\dot{m}_c$) => V = 1 m/s

$\dot{m}c = \rho \bullet V \bullet Afr$
T = 303 k -> ρ = 1,151416. Kg/m^3 ; Cp= 1,007 kj/kg . K

Afr = 50 cm x 55 cm = 0,275 m^2 Cp = 1007 J/Kg . K

$\dot{m}c$ = 1,151416 Kj/m m/s . 0,275 m^2

$\dot{m}c$ = 0,316 Kg/s

T1 = 343 K ; ρ = 978,47 Kg/m^3 ; Cp = 4189 J/Kg . K

$$\circ > \varepsilon = \frac{\dot{m}c \,.\, Cc\,(Tco - Tci)}{\dot{m}h \,.Ch\,(Thi - Tci)} = \frac{\dot{m}c \,.\, Cc\,(T4 - T3)}{\dot{m}h \,.\, Ch\,(T1 - T3)}$$

$$= \frac{0,316\frac{kg}{s}.1007\frac{j}{kg}.\, k(315-303)k}{\dot{m}h \,.\, 4189\frac{j}{kg}.\, k \,.\, (343-303)k} = \frac{3818,544\ j/s}{\dot{m}h \,.\, 167560\ j/kg}$$

$$0,3 = \frac{3818,544\ j/s}{\dot{m}h \,.\, 167560\ j/s} => 50268\ \dot{m}h = 3818,544$$

$\dot{m}h$ = 0,075 kg/s

From the above calculations, in order to get optimal results, a clove dryer simulation tool was redesigned by adding a flowmeter and valve, replacing the previous 3/8 inch diameter pipe, to 1/2 inch diameter. This clove dryer simulation tool uses a pump with a maximum capacity of 30 l/ min.

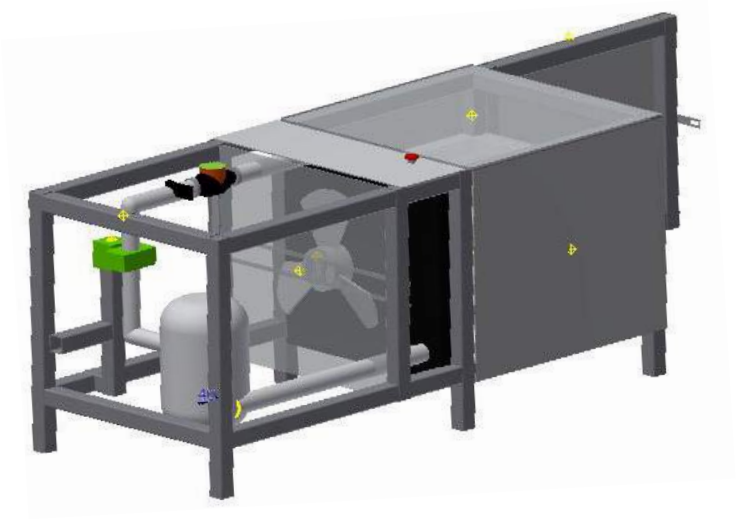

Figure 2. redesign of clove dryers

3.2. Performance of Clove Dryer

The performance of radiator as a source of the clove dryer has been tested experimentally. The water as the working fluid has been heated by the heater in the reservoir tank and will be circulated to the radiator by a pump with a flow rate of 30ℓ / min. The mass flow rate of water inlet radiator are measured using a flow meter which the speed control using a valve. The heat transfer process of the radiator is carried out by forced convection using air blowing from the fan with a flow rate of 1 m/s. The temperature of the water enters the radiator, exits the radiator, the air temperature before the radiator, and the air temperature after the radiator is measured using a thermocouple. The test results on the temperature of radiator exhaust heat are shown as table 2 and table 3 below

Table 2 Performance of Dryer ($\dot{m} = 0.09\ kg/s$)

NO	Time (minutes)	T1 (K)	T2 (K)	T3 (K)	T4 (K)	m air (kg/s)	qc (Watt)	Dryer Effectiveness (ε)
1	0	354.5	332.6	302	316.7	0.097	4504.565	0.28
2	5	353	331.3	302	315.4	0.097	4122.055	0.26
3	10	335	329.4	302	313.1	0.098	3437.767	0.34
4	15	332.3	327.2	302	312.6	0.098	3287.734	0.35
5	20	335.4	329.7	302	313.3	0.098	3497.652	0.34
6	25	333	328.3	302	314.2	0.098	3766.237	0.39
7	30	332.1	327.4	302	314.5	0.098	3855.437	0.42

Table 3 Performance of Dryer ($\dot{m} = 0.18\ kg/s$)

NO	Time (minutes)	T1 (K)	T2 (K)	T3 (K)	T4 (K)	m air (kg/s)	qc (Watt)	Dryer Effectiveness (ε)
1	0	343	338.3	302	317.2	0.186	4650.773	0.37
2	5	336.2	333.4	302	316.6	0.187	4475.037	0.43
3	10	333.3	330	302	316	0.187	4298.485	0.45
4	15	332.1	328.9	302	314.7	0.187	3914.486	0.42
5	20	328.9	326	302	313.9	0.186	3676.785	0.44
6	25	327.1	324.6	302	313	0.186	3407.959	0.44
7	30	326	323	302	312.9	0.186	3378.023	0.45

From the results of these calculations, the graphical analysis of the radiator performances shows in Figure 3, Figure 4 and Figure 5. The results show that the radiator output temperature on the air side (T4) is initially high at the beginning, because the radiator has just began to work dissipate the heat into the environment, so that the heat dissipation of the radiator was not too effective. The temperature then will tend to be stable in the range of 314 K for both mass flow rates after 25 minutes. This shows that the heat dissipation process from the radiator has run quite well, where the heat from the water will be transferred into the environment by the radiator so that the water temperature will tend to be stable. These were similar to the radiator output temperatures on the water side (T2) where at the beginning it's initially high then it will tend to stabilize in the range of 329 K after 18 minutes work for both mass flow rates.

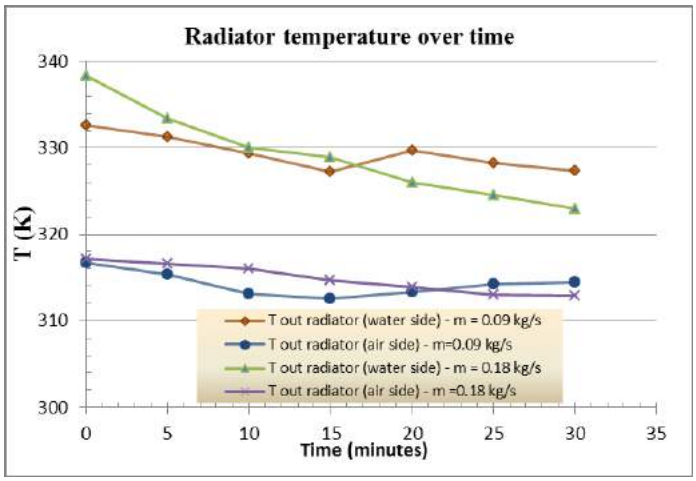

Figure 3. Radiator temperatures over time

The results of the calculation of the heat transfer rate on the air side (qc) over time shows that at the beginning the heat transfer rate is high and will tend to decrease. This is in line with the outside radiator temperature on the air side which tends to decrease compared to the start for both of mass flow rates. The heat transfer rate will tend to be stable after the 25th minute with an average qc of 3781.64 watts for the mass flow rate of 0.09 kg/s and 3971.65 watts for mass flow rate 0.18 kg/s. The maximum heat transfer rate values were 4680 watts for the hot water mass flow rate of 0.18 kg/s. From the analysis shows that the effect of mass flow rate to the performance of radiator's heat transfer was quite significant. The heat transfer rate of air-side radiator will higher with the higher of mass flow rate.

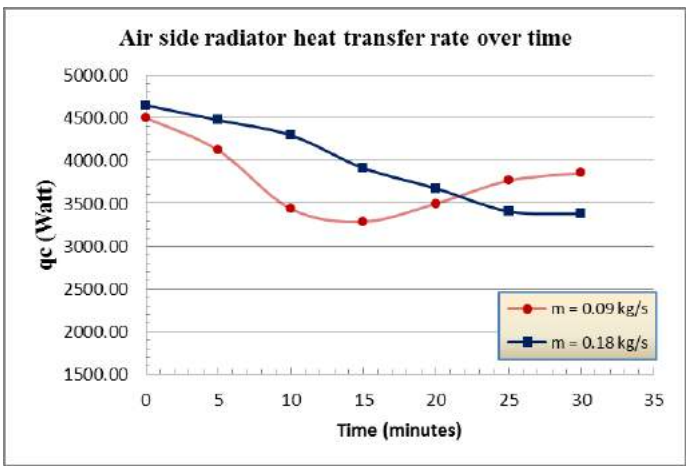

Figure 4. Heat transfer rate of radiator over time

The results of the radiator's effectiveness (ε) as the source of the clove dryer over time showed a tendency to increase. This can occur because the circulation process and heat dissipation of the radiator goes very well. The performance of radiator to circulate the hot water was quite good enough. Radiators are able to produce exhaust heat that is significant enough to be used as a heat source for drying. The average effectiveness of the radiator is 0.34 for the mass flow rate of hot water 0.09 kg/s and 0.43 for the mass flow rate of hot water 0.18 kg/s. From this analysis shows that the average radiator's effectiveness were higher with

the higher of mass flow rate. This was similar with the air-side heat transfer rate of radiator.

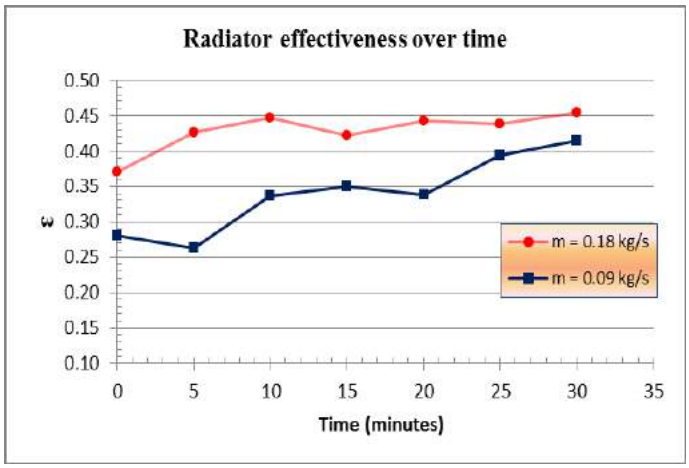

Figure 5. Radiator effectiveness over time

This clove dryer was also tested with a load of 1 kg of wet clove. The drying time for 1 kg clove is 5 hours 30 minutes with a fluid flow rate of 0.18 kg/s. The average heat dissipation of the radiator is 314.87 K with the effectiveness of 0.42. For the fluid flow rate 0.09 kg/s, the drying time of 1 kg clove is 6 hours with the average heat of 314.54 K and the effectiveness of 0.33.

Figure 6. Clove before drying with the dryer tools

Figure 7. Clove after drying with the dryer tools

4. CONCLUSION

From the analysis of thermal radiator's performances shows the effect of mass flow rates to thermal radiator's performances quite significant. The results of the redesign of the clove dryer using a radiator as a heat source can run well. The system produces the heat exhaust with average temperature 314.87 K with the effectiveness of 0.42 for the water mass flow rate 0.18 kg/s, and the average temperature 314.54 K for the

water mass flow rate 0.09 kg/s with the effectiveness of 0.33. The clove dryer using a radiator as the heat source also can drying the clove properly. For the load of 1 kg wet clove, the drying time are 5 hours and 30 minutes for the variation of water flow rate 0.18 kg/s and 6 hours for the water mass flow rate 0.09 kg/s.

5. ACKNOWLEDGEMENT

The authors would like to acknowledge The Directorate of Research and Community Service, Ministry of Research, Technology, and Higher Education Republic of Indonesia for funding this research. Authors also like to thank full to the research team and all the staff of Mechanical Engineering Department of Bali State Polytechnic for the support.

6. REFERENCES

[1] Murugesan M.P. and Balasubramanian R, "The effect of mass flow rate on the enhanced heat transfer charactristics in a corrugated plate type heat exchanger", Res. J. Engineering Sci, vol 1 (6), pp. 22 – 26, 2012.
[2] V. Salamon, D. Senthil kumar, S. Thirumalini, "Experimental investigation of heat transfer characteristics ofautomobile radiator using tio2-nanofluid coolant", IOP Conf. Ser.: Mater. Sci. Eng. 225 012101
[3] Sabharwall Piyush, Vivek Utgikar, Fred Gunnerson "Effect of mass flow rate on the convective heat transfer coefficient: analysis for constant velocity and constant area case", Nuclear Technology, vol 166:2, pp. 197-200, DOI: 10.13182/NT09-A7406 [4] K. H. E. Kroemer and E. Grandjean, *Fitting The Task To The Human, Fifth Editione A Textbook Of Occupational Ergonomics*. London: CRC Press, 2009.
[4] Mirmanto, Emmy Dyah Sulistyowati, I Ketut Okariawan, "Effect of mass flow rate on dryer room radiator pressure drop and heat transfer", Applied Mechanics and Materials, vol. 836, pp. 102-108, 2016.
[5] Trivedi P.K, N.B.Vasava, "Study of the effect of mass flow rate of air on heat transfer rate in automobile radiator by CFD simulation using CFX", International Journal of Engineering Research & Technology (IJERT), vol 1 (6), 2012.
[6] Wiryanta, I.K.E.H "Studi eksperimental unjuk kerja radiator sebagai sumber energi panas pada rancang bangun simulasi alat pengering." LOGIC. Jurnal Rancang Bangun dan Teknologi, vol. 17, no. 2, Juli 2017.
[7] Incropera F P, D P Dewitt, "Fundamentals of Heat and Mass Transfer Seventh Edition", New York: John Wiley & Son, 2011..
[8] Holman JP, "Heat Transfer Sixth Edition", Singapore: McGraw-Hill Company, 1986.
[9] Johanes S., F. Eko Wismo Winarto, "Studi efisiensi termal proses pengeringan cengkeh pada alatpengering yang memiliki lima tingkat tray." Prosiding Seminar Nasional Teknologi Terapan SV UGM 2016, pp 954 - 958.

LOGIC
Journal of Engineering Design and Technology
Vol. 19 No.1 March 2019 ; p. 14 - 19

p-ISSN : 1412-114X
e-ISSN : 2580-5649
http://ojs.pnb.ac.id/index.php/LOGIC

DESIGN OF ERGONOMIC WORK DESK FOR WORKBENCH PRACTICUM

Kurnia Dwi Artika [1)], Rusuminto Syahyuniar [2)], Adhiela Noer Syaief [3)]

[1,2 3)] Mechanical Engineering Department, State Polythecnic of Tanah Laut, South Kalimantan

Corresponding email :
[1)]kur.artika@gmail.com

Abstract. Polytechnics as vocational education that applies more mastery of ability in the field of technology by prioritizing 70% practicum and 30% theory. As for workbench practicum, it is one of the basic practicum in the Automotive Engineering Department. This practicum contains basic mechanical work that is within the scope of conventional machining. The problem is the ineffectiveness in conducting the practicum process, where facilities and infrastructure are minimal and far away from the reach of work equipment, thus inhibiting the bench work practicum process. So it needs to be conducted on ergonomic workbench by determined good body position or movement based on the RULA value. The results of the application of ergonomic bench design workbench related that with setting equipment in one table, worker position, and the use of equipment had a value of RULA was 4.

Keywords : Ergonomic, Workbench, Vise, Effectivity, RULA

1. INTRODUCTION

Automotive engine is one of the study programs at State Polytechnic of Tanah Laut. Automotive engine study programs continue to strive to organize and develop vocational education that is in accordance with the competencies in the field of mechanical engineering and automotive to be able to meet the needs of industry in Tanah Laut District. as a vocational education, automotive engine study programs have a curriculum of 70% practicum and 30% theory. This aims to make students more skilled in working skills [1]

One of the practicum in the automotive engine study program curriculum is workbench practicum. Workbench practicum is a basic practicum in the field of mechanical engineering. This practicum is usually conducted in the first semester of lecture.

In various studies, there has been an influence of the application of ergonomics in the world of work, such as improving work performance due to the implementation of ergonomics in workbench practicum at 5.74% compared to not applying ergonomics, namely in the assessment of aspects of working time, flatness, sophistication, conformity fineness of workpiece [2].

Sutarna (2013), the research has used the foundation for workbench practicum by measuring the workload through the pulse of a minute to the height of the vise, the results has revealed that the use of the foundation was very effective in increasing comfort, health and safety of students in workbench practicum [3].

There are problems such as the wrong position in practice, the lack of equipment so there is a waiting time (turns) in the use of tools, and remote equipment coverage, so an ergonomic work desk design is needed to accommodate students in practicing workbench in groups without having to move places, because the workpiece and equipment will be in one table in the middle to facilitate the process of working the bench.

2. METHODS

The stages to be conducted in this study were as follows Figure 1:

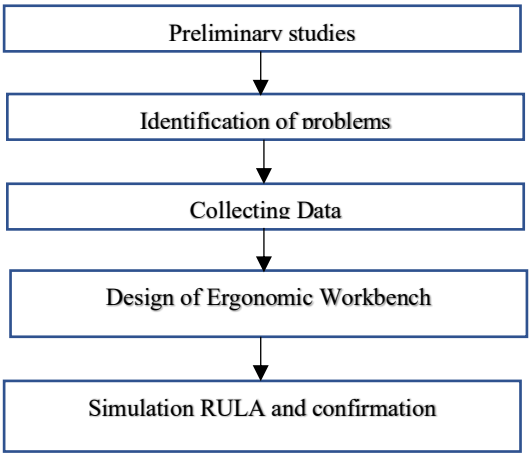

Figure 1. Flow Diagram

After conducting the work desk design then the next work desk design is conducted in accordance with the results of observations of students who did practicum and workbench practicum activities to be conducted. It concerned about the dimensions, shape, work corner of the bench, workbench material, effectiveness, and RULA (Rapid Upper Limb Assessment) [4].

The method of evaluating to person's body and muscle parts during activities measured by the level of injury risk. Such as workplace accidents, injuries, the best position and ergonomics. This is influenced by [5]:

a. The work position is not natural
b. Repeat work on one type of muscle
c. Excessive use of energy
d. Static work position
e. Contact occurs with body parts with the environment or work equipment
f. Method / method of work
g. Working hours are too long

3. RESULTS AND DISCUSSION

Data retrieval was conducted in the Workshop, by measuring student body posture, along with height measurement data Table 1.

Table 1. Student Body Height Data Practicum Workbench

Initials Name of Students	Height body	Armpit height	Upper arm length	Forearm length	Wrist height
	a	**b**	**c**	**d**	**e**
IS	175	133	33	30	81
MR	171	134	31	28	81
AM	157	123	28	28	77
HD	160	123	28	25	78
AF	175	133	31	29	86
DN	170	134	31	28	85
DS	168	132	30	27	84
FZ	160	126	26	26	80
SP	163	127	27	25	78
AN	166	129	28	29	80
AR	167	120	33	27	78
FT	170	130	26	30	85
FR	174	134	30	30	84
Fikri	178	135	30	29	84
AG	166	127	28	30	80
EW	175	138	30	30	83
BA	170	134	28	26	84
FM	172	128	26	26	80
IK	166	130	28	28	84
RA	161	120	26	24	80
Mean	**168.20**	**129.50**	**28.90**	**27.75**	**81.60**

(source: research data, cm)

The following is a method of measurement conducted on students body posture, as in Figure 2, for example a is for height, b for armpit height and so on.

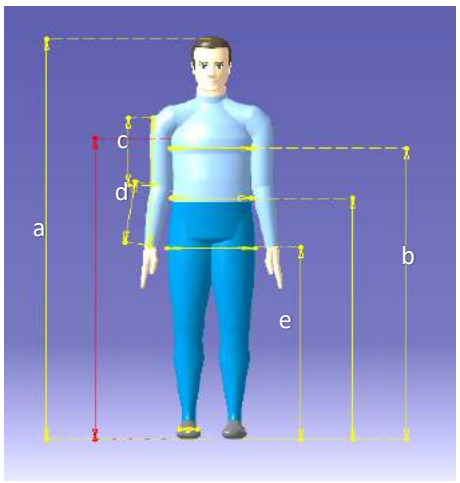

Figure 2. Methods of Student Body Posture Measurement

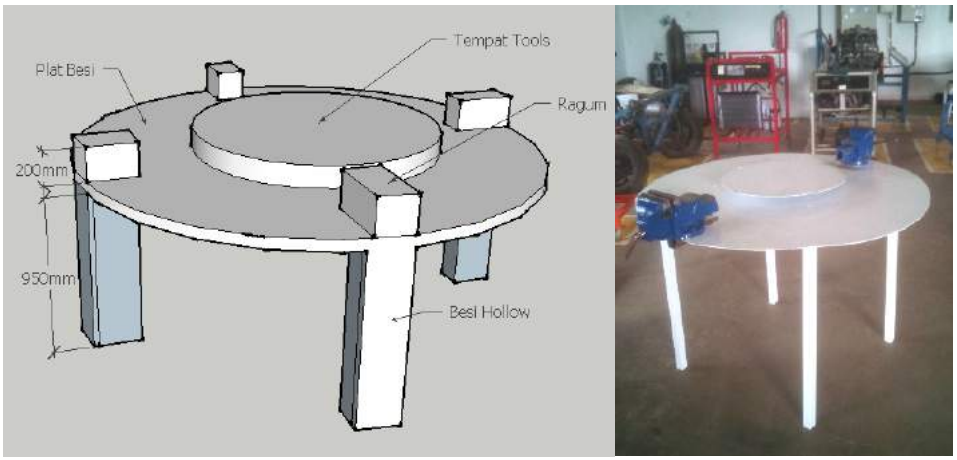

Figure 3. Design of Ergonomic Workbench

With the average height of the student doing the workbench practicum was 168.2 cm, with the upper arm length of 28.9 cm, it could be determined the height of the hollow metal as the workmanship was 95 cm, with a height of 20 cm. So the total height of the vagus was 115 cm, according to the lower arm angle of 65 degrees, from arm straightness with RULA 2 score, and max workbench capacity for 4 students.

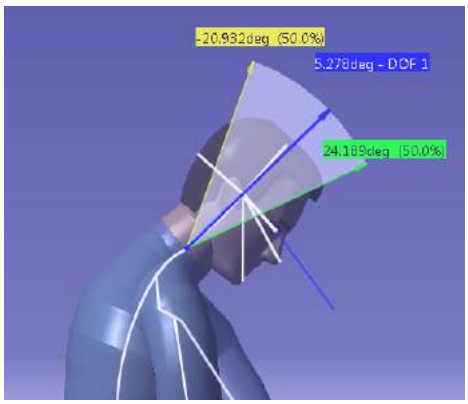

Figure 4. Neck and Head Position

In Figure 4, could be seen the angle for the head position slightly looking down at the vise and the work process in hand, getting the RULA 2 score.

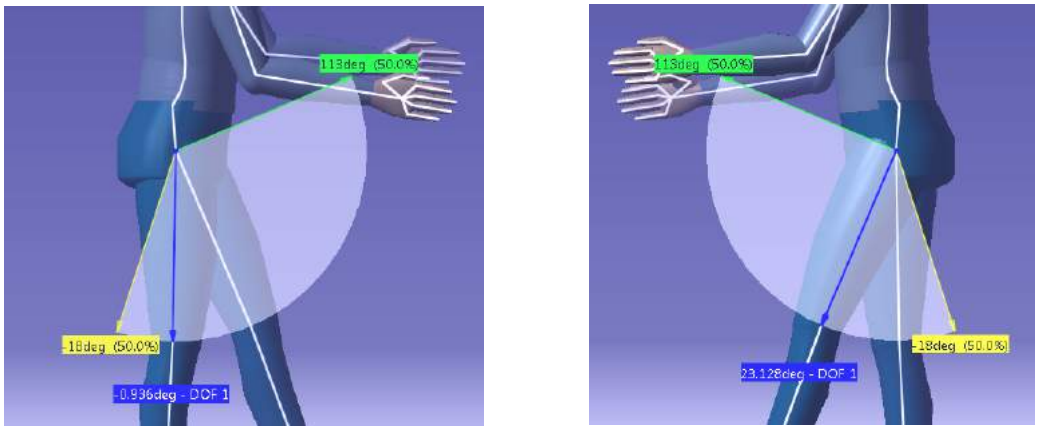

(a) Right (b) Left

Figure 5. Leg Position (a) Right; (b) Left

For the position of the foot as shown in Figure 5, in conducting the practicum, the left foot was forward for 23 degrees, and the right foot was backward by 0.9 degrees. The pedestal was charged to the left leg, because the movement of the hand muscles was on the right. It conducted in order to be strong in the process of thinking or cutting metal, the results will be maximum and accurate.

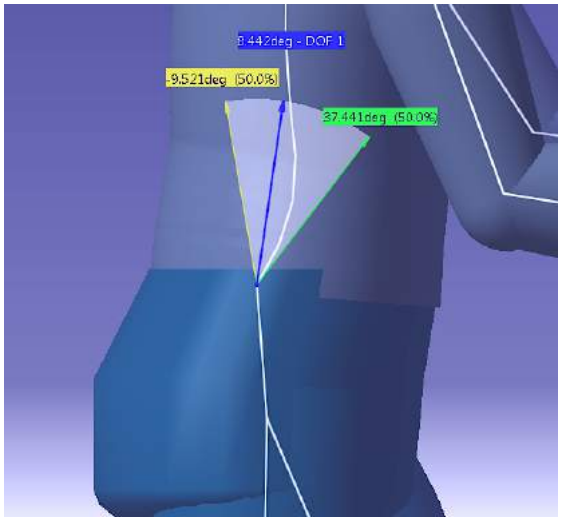

Figure 6. Wrist Position

Seen in Figure 6, the back position was slightly bent, around 6 degrees, so that the RULA score was 2.

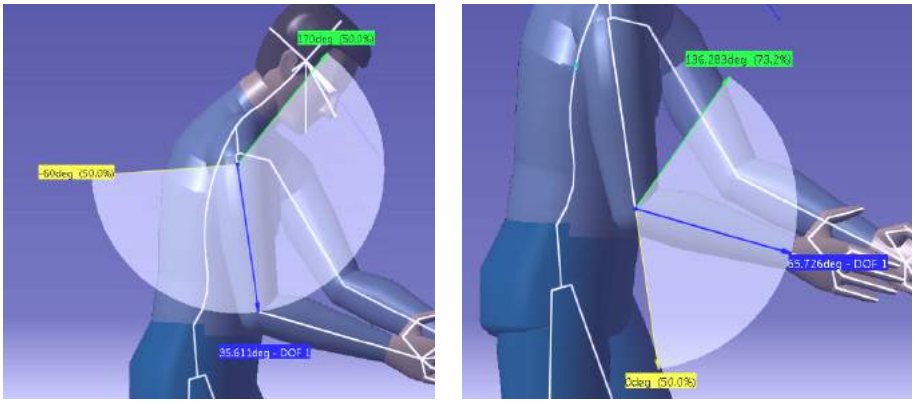

(a) upper arm (b) forearm

Figure 7. Position of the Right Hand (a) Upper arm ; (b) Forearm

In Figure 7, the position of the upper right arm got a RULA 2 score, and the RULA score forearm 1. This attitude was in accordance with the bent back movement, so the work wasn't too heavy and is highly recommended in the process of implementing workbench practicum.

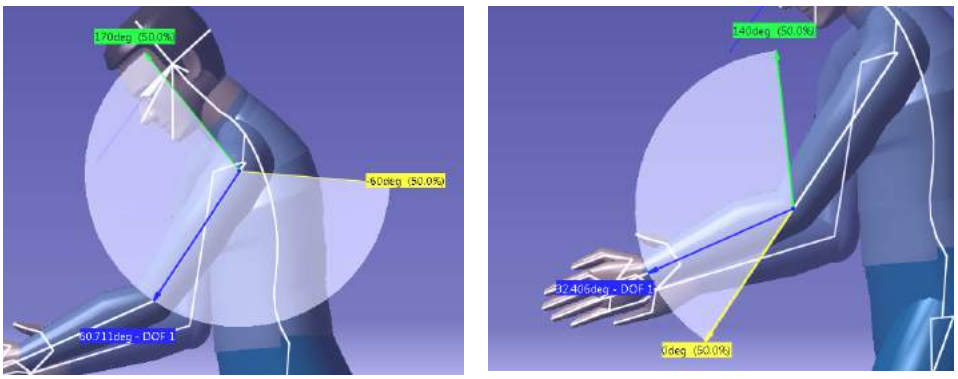

(a) Upper arm (b) Forearm

Figure 8. Position of the Left Hand (a) Upper arm ; (b) Forearm

In Figure 8, the position of the upper left arm got a RULA score of 3, and the forearm score of RULA 2. This attitude were still permitted to perform the workbench practicum process, because the position was rather straight from the upper arm to reach the corner of the equipment while holding and as a guide. so the workload is large and the angles formed were also large, with repetitive work. Seen in Table 2.

Table 2. RULA score before and after applying workbench ergonomic

RULA score	Ergonomic workbench	
Position	Before	After
Neck	**4**	**1**
Trunk	2	2
Wrist	2	2
Left Upper arm	3	3
Left Forearm	2	2
Right Upper arm	2	2
Right Forearm	1	1
Leg	1	1
Total Score	**6**	**4**

4. CONCLUSION

The ergonomic design of the workbench had dimensions of 115 cm, table diameter of 120 cm, and diameter of the equipment 50 cm that could be rotated, with the calculation of RULA was 4 and workbench maksimum capacity of 4 students.

5. ACKNOWLEDGEMENT

The author would like to thank the director of the State Polytechnic of Tanah Laut who has provided funding for DIPA (PDP research) and P3M as research organizers who provide direction and motivation for the smooth running of our research.

6. REFERENCES

[1] K. D. Artika, *Panduan Praktikum Kerja Bangku*. Pelaihari: Politeknik Negeri Tanah Laut, 2017.
[2] T. A. Wibowo, Solichin, dan A. Martiningsih, "Meningkatkan Prestasi Kerja Bangku Dengan Penerapan Ergonomi," *Tek. Mesin*, vol. 22, no. 1, hal. 1–7, 2014.
[3] I. N. Sutarna, "Analisis Ketinggian Ragum Terhadap Beban Kerja Mahasiswa Praktek Kerja Bangku Di Bengkel Teknologi Mekanik Politeknik Negeri Bali," *LOGIC*, vol. 13, no. 3, hal. 82–87, 2013.
[4] A. R. Sutalaksana dan J. H. Tjakraatmadja, *Teknik Tata Cara Kerja*. 1979.
[5] I. M. L. Batan, *Desain Produk*, Pertama. Surabaya: Guna Widya, 2012.

LOGIC
Journal of Engineering Design and Technology
Vol. 19 No.1 March 2019 ; p. 20 - 24

p-ISSN : 1412-114X
e-ISSN : 2580-5649
http://ojs.pnb.ac.id/index.php/LOGIC

Analysis Of The Effect Of Temperature On Tire's Durability On Engkel Truck Vehicle

I Wayan Suastawa [1], Ida Bagus Putu Sukadana [2]

1) Department of Mechanical Engineering, Politeknik Negeri Bali Bukit Jimbaran, P.O. Box 1064 Tuban-Badung, Bali
2) Department of Mechanical Engineering, Politeknik Negeri Bali Bukit Jimbaran, P.O. Box 1064 Tuban-Badung, Bali

Correponding email [1] : asta782002@yahoo.com

Abstract. Tires are a very important component of a vehicle, a variety of charges are imposed on the tires when the vehicle is stationary or moving. The various loading styles directly rest on the air trapped in the tire, and cause the rise of pressure to flow in accordance with the magnitude of the various forces it receives. The rise in tire pressure mainly occurs when the vehicle is in motion, where the tire gets a compressive force from the constant load of the vehicle and the shock load due to the road contour. High pressure and rising and falling causes heat on the tire which then heat is moved to the rubber tire layer. Besides also because of the heat when the surface of the tire tread rub against the road during acceleration and braking.

Assuming that heat is the main cause of tire damage then this study will try to analyze the influence of tire rubber temperature on the ability of work to withstand the air pressure in the tire. The loading received by the tire rubber coating is assumed to be the same as the tensile test that will be applied to the tire when used. This tensile test will be carried out on the rubber tire layer by heat treatment before it is tested. Temperature treatment starts from a temperature of 30 until 110 with a range of 20 degrees, with the expected stress value and the best strain obtained at that temperature range. The tire samples used in this study are two of the most used tire brands on ankle truck trucks which are the most widely used truck types.

With tensile test the tire performance is generally very good at low temperature up to 70 degree temperature, above 70 degree temperature tire performance began to decrease due to the increased strain on the tire material so that the ability to resist high pressure by the pneumatic force of the wind inside the tire decreased relative Against the increase in tire temperature.

Keywords : Vehicle tires, loading style, tensile test..

1. INTRODUCTION

Tires are a component that needs attention in a vehicle. A variety of loading styles are worn on the tires, both when the vehicle is in motion or still. The three forces acting on the tire are normal or vertical forces caused by the weight of the vehicle, the longitudinal force due to the acceleration or braking force and the lateral or lateral forces caused by the vehicle's centrifugal force [2]. The force causes damage along with the duration of use and when it gets excessive force and shock force it will cause the rupture of the tire. Various kinds of excessive force that may occur in the tire caused by various things such as vehicle load is too high, road damage, collision with uneven road surface, and foreign objects that can stick on the tires that cause tire pressure leak [1].

In the vehicle of goods or material dimension of vehicle and tire become limiting ability of vehicle transport so often at stake its ability to economical value of vehicle transport become feasible. For example a medium-sized truck carrying 2-axis 2-axis of sand that should carry 5 tonnes of sand today with an economical calculation is used to carry sand weighing approximately 12 tons [6]. This is what causes the rapid destruction of vehicle components, especially tires or the occurrence of tire breaks in transit [5]. Based on experience passed on from generation to generation, truck drivers try to overcome and anticipate the breaking of tires and the rapid wear of

tires by way of stopping the roadside to lower the temperature of the tire known as "Ngeban". If it is felt the tire temperature is cold enough then the truckers continue the journey. In a roadside survey conducted on Jalan Mahendradatta there are many trucks loaded with sand stopping around Lembeng Beach with a duration of half to 1 hour. From the interview it is known that they are cooling the tires (ngeban) as mentioned above, from the interview also found that if ngeban not done then the tires become too hot and can cause tire breaks and fast tire wear. From interviews also obtained the long use of tires and brands of tires are often used.

Theoretically the breakdown or breakup of the tire is due to the amount of air pressure inside the tire due to the various forces that rest on the air captured in the tire. Pressure and force that rests on the air trapped in the tire increases the tire pressure in all directions equally [4]. Pressure or excessive force does not necessarily cause a tire break even though it is pressurized above the tire specification capability. However, due to the presence of lateral and longitudinal forces when moving or rotating, the pressure on the tire changes and causes a change in temperature. The pressure change accumulates and is proportional to the length of rotation or movement of the tire without stopping, the accumulation causing heat or temperature changes in the air in the tire, which then moves on the tire rubber layer [2]. This heat damages the tire, causing wear and tear [3]. Increased tire temperature in addition to the ups and downs of air pressure in the tire is actually also caused by the friction of the tread of the tread with the road during acceleration and braking. The only way to cool the tire back is to stop the roadside or silence until the temperature of the tire back cold. Based on the background above this study takes the theme of analyzing the effect of temperature on tire resistance. In this study a study of the effect of temperature on durability and tire elasticity. From this study will get the value of a certain temperature where the tire has the best performance capabilities. The object of this study is the most widely used tire on the truck Engkle which is the most used middle-class commercial truck in the area of Bali.

Based on the above background, then taken the formulation of the problem as follows:

1. How does temperature influence truck tire performance with tensile test?
2. What is the best working temperature of each tire brand that is widely used in Engkel trucks?

2. METHODS

The method used is to test the object directly studied in this case is in the form of an armor truck tire. The tires are sampled in the form of Engkel truck tires with the size of alloy wheels 60 ring 16 with the size of bias 750 tires brand Bridgestone and Gajah Tunggal brand. As shown in Figure 1, each tire will be split / cut off the left and right blanket into 5 specimens. The total specimens were 10 specimens.

On a predetermined day the data will be taken in the form of stress and strain of each specimen by first providing heat treatment by inserting it into the microwave and setting the microwave heat degree in accordance with the specimen's planned heat. The first specimen is heated to a temperature of 30 or more to be obtained after the specimen is tested at that temperature. Furthermore, after checking the specimen heat is then mounted on a tensile test choke and measured tension and strain. And so on until all the specimens get heated and tested from a temperature of 30 to 110 degrees Celsius with an increase of 20 degrees.

After all data obtained then input and tabulation of data in microsof excel to obtain the graph and compare one graph with other graph. From the graph it can be seen the tendency of the graph line to further narrated in the analysis results.

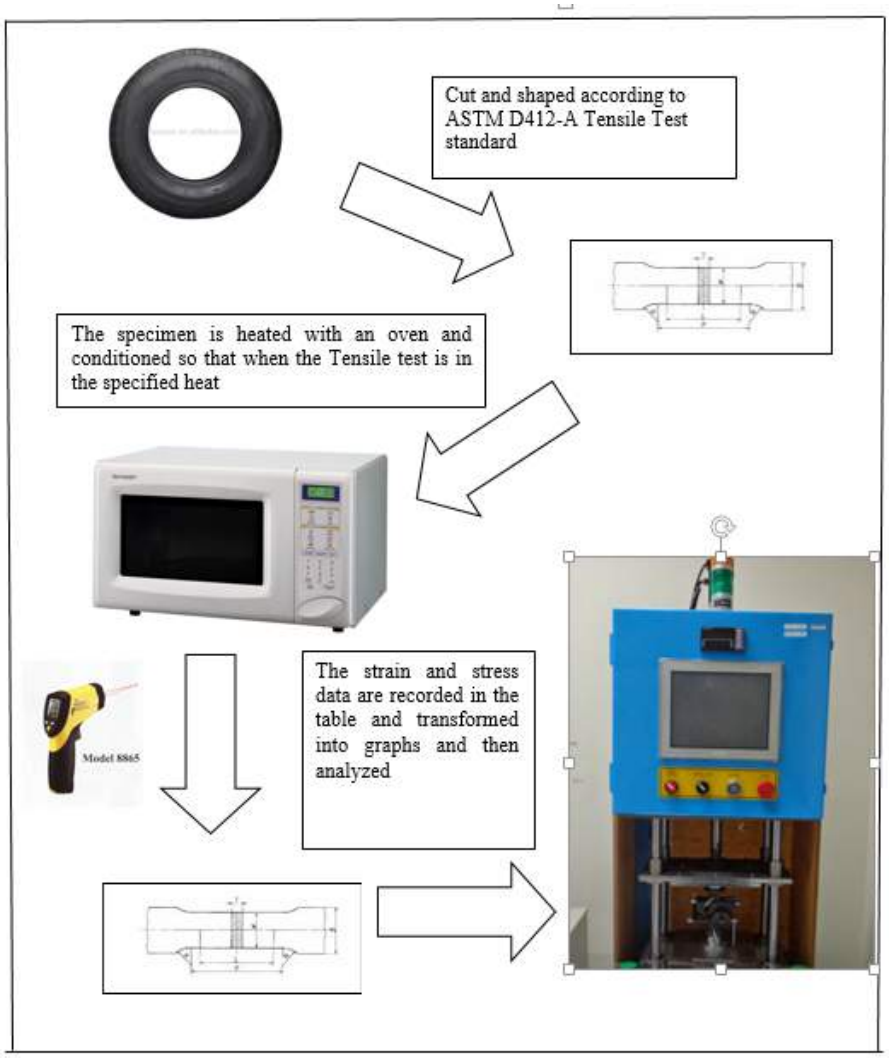

Figure 1. Test Flow

3. RESULTS AND DISCUSSION

From 5 specimens on each tire brand, 10 data were recapitulated as shown below:

Table1. Recapitulation of Tension and Strain

No	Temperature (°C)	Tension (Kgf/mm^2)		Strain mm/mm	
		Tension No A	Tension No B	Strain No A	Strain No B
1	30	0.6	0.5	1.9189	1.831
2	50	0.3	0.3	1.9159	1.8059
3	70	0.3	0.3	1.9395	1.8177
4	90	0.3	0.3	1.9895	1.8959
5	110	0.2	0.2	2.1294	1.9294

From the table above then transformed into a graph as shown in Figure 2

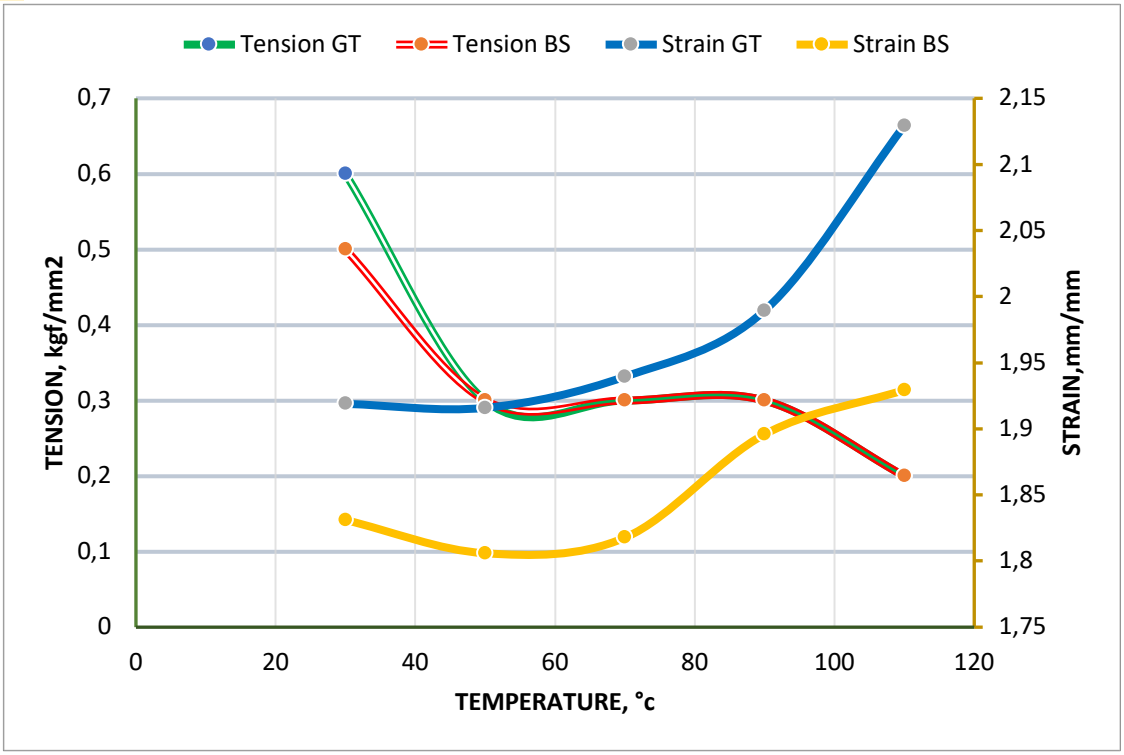

Figure 2. Graphics Effect of temperature on tension stress and strain

From the graph, the tire strain B (BS) is relatively lower than the A (GT) tires at all temperatures. While in the second tire voltage has almost the same value only tire voltage A (GT) at a temperature of 30 ° C has a higher voltage but at other temperatures the same value with tire B (BS). From the graph above it can also be seen from the strain perfomance both tires are relatively good at low temperatures but decreased at temperatures above 90 ° C seen from the stress while viewed from the strain, the performance of both tires decreased at a temperature of 50 to 60 ° C.

4 Conclusion

The conclusions that can be drawn from the results of this study are as follows:

1 With tensile test the tire performance is generally very good at low temperatures up to 70 degrees, above 70 degrees the performance of tires began to decline due to the increased strain on the tire material so that the ability to resist high pressure by the pneumatic force of the wind inside the tire decreased relative to the increase Tire temperature.

2 For the best performance A (GT) tires at low temperatures up to 70 degrees, as well as B (BS) tires, although generally at low temperature the performance of B (BS) tires is relatively better than A.

5. ACKNOWLEDGEMENT

The authors would like to thank the Directorate General for Research Strengthening and Development, Ministry of Research, Technology and Higher Education, Republic of Indonesia which has funded this research

6. REFERENCES

[1] Prasetya Hari Akademi Teknologi Kulit.Yogyakarta. Arang Aktif Serbuk Gergaji Bahan Pengisi Untuk Pembuatan Kompon Ban Luar Kendaraan Bermotor. Jurnal Riset Industri, Vol. VI. Palembang. 2012.
[2] Ian Hardianto Siahaan, Ninuk Djonoadji, Amelia Sugondo. Analisa Gaya Pada Roda Kendaraan Pada Berbagai Kecepatan. Product Innovation and Development Centre Petra Christian University. Jurusan Teknik Mesin, Fakultas Teknologi Industri-Universitas Kristen Petra. Laboratorium Pengaturan dan Uji Konstruksi, Universitas Kristen Petra Surabaya .2006
[3] Rahmaniar, marlina.. Pengaruh Ukuran Partikel Nano Sulfur Terhadap Sifat Fisis Karet
[4] Jurnal of Industrial Reasearch, Komponen Kendaraan Bermotor., Vol. IV. Jakarta.
[5] Wikipedia, 2012, Ban, diakses dari http://id.wikipedia.org/wiki/Ban
[6] Wikibooks.org. wiki. Moda. Transportasi/Moda. Transportasi Jalan diakses dari http://id.wikipedia.org/wiki/Ban

LOGIC
Journal of Engineering Design and Technology
Vol. 19 No. 1 March 2019 ; p. 25 - 33

p-ISSN : 1412-114X
e-ISSN : 2580-5649
http://ojs.pnb.ac.id/index.php/LOGIC

TELLURIUM EFFECT ON ASTM A 220 GRAPHITE MALLEABLE CAST IRON

Mohammad Nur Hidajatullah[1)], Achmad Sambas[2)], Khansa Sarah Puspita.[3)]

1,2,3 Foundry Engineering Departement,
Politeknik Manufaktur Bandung,

Jalan Kanayakan Nr.21,
Bandung, West Java, Indonesia

Correponding email :
1) mnurhidajat@gmail.com
2) sambas.achmad@gmail.com
3) sarahkhansa@gmail.com

Abstract. Malleable cast iron is an variant of cast iron which has rose-shaped graphite, the appearance of graphite due to the process of heat treatment. In general, a Boron element is needed in making the material. In this study, Tellurium was used as a substitute for boron. The main objective of the investigation was to determine the effect of tellurium composition on graphite microstructure and the mechanical properties of malleable cast iron. Variations in tellurium are added to the ladel, cast into specimen molds. Each specimen was subjected to annealing heat treatment at 900^0C and held for 10 hours. Then each specimen was tested in composition, microstructure, and hardness test. The test results showed that there was an effect obtained from the addition of tellurium to microstructure and hardness. Graphite structure increases from 2% to 6.5% and hardness increases from 38 HRc to 43 HRc.

Keywords: Malleable Cast Iron, Tellurium, Annealing.

1. INTRODUCTION

Malleable cast iron is cast iron which has middle class mechanical properties compared to ductile cast iron or other cast iron. This material provides good ductlity but has a higher toughness value than gray cast iron. Special application of this material is capable of being used in a bent or bent position but does not cause cracking. This material has good characteristics making it suitable for making pipe fittings, beam adapters, clamps, tools, connectors, and many more [2] [7].

The percentage of Malleable cast iron usage is equal to ductile cast iron. Especially for thin-wall castings, toughness exceeds ductile iron [6].

The hardness of ferritic malleable cast iron is expected to be around 110-156 HB, around 62–82 HRB (below 20 HRC) [8].

Figure 1 Some applications for using malleable cast iron

The process of making malleable cast iron goes through several stages, including alloy design, metal casting, and analing process. As for the metal casting process, the material is cast into white cast iron. Tellurium in malleable cast iron is usually added in the range 0,0005% to 0,001% to suppress mottle (graphite spots). Tellurium is a carbide stabilizer and has a stronger influence than bismuth during the freezing process. Tellurium was added to the ladel to ensure cast iron became a full white iron structure. But tellurium also has a strong influence on slowing down the annealing process in a content of more than 0.003%. Less than 0.003%, tellurium

has a smaller influence on the annealing process, but it already has an influence on mottle control. Tellurium will be more effective if added with bismuth. In previous studies according to E.G Mekhanicheva: Tellurium was added when the liquid was in the ladle with a percentage of 0.01% - 0.6%. As a result, tellurium makes objects white and according to the study, the percentage of tellurium increases, giving rise to inclusion of graphite with increasing size, but the quantity decreases [7].

The purpose of this study was to determine the effect of Tellurium with a smaller content on Graphite Malleable Cast Iron ASTM A 220.

In this research, tellurium will be included in the print with a low composition of 0,0005% - 0,0025%. The hypothesis in this study is that tellurium will increase the size of graphite.

Malleable cast Iron is a type of cast iron that has a white structure, which has a very fine graphite element so that the distribution of Carbon elements is more evenly distributed and easily formed. Malleable cast Iron is divided into two types, namely: Whitehearth, Blackhearth, these names are terms in accordance with the microstructure of cast iron [3].

The process was originally made of white cast iron by applying a heat treatment. The heat treatment applied to white cast iron is generally annealed. By treating this Fe3C carbide phases will decompose to ferrite and graphite. Graphite formed is not shale or round, but in the form of clumps of graphite that do not have sharp edges.

The process of making malleable cast iron through two stages, namely metal casting and heat treatment. The first stage is the metal casting process. Iron in cast becomes white cast iron.

After finishing the metal casting process is complete, then the next step is the treatment process. The heat treatment or heat treatment process has three stages, namely heating, holding, and cooling. The heating process is the material heated at a certain temperature, then held until the homogeneous structure and finally cooled to a certain cooling rate to obtain the desired micro structure.

Heat treatment of cast iron can determine the final structure of this iron. There are two basic stages for forming this iron. In the first stage, iron carbide is broken down into austenite and graphite. In the second stage, austenite is converted to pearlite, ferrite, or both alloys. Even though there is a difference in composition between ferritic and perlitic castings, the difference mainly in the heat treatment cycle. To form a ferritic structure is needed to decrease the temperature in the range of 3 to 10 ºC / hour through eutectoid transformation in the second stage. This is needed to make a complete change from austenite to ferrite. When ferritic forging is made, the scheme used is different, the main goal is to achieve eutecoid transformation to convert austenite to pearlite.

In the manufacture of Ferrtitic-Malleable Castron there are 2 stages of Graphite formation; First-Stage Graphitization & Second-Stage Graphitization. For the manufacture of Pearlitic-Malleable Cast Iron, the heat treatment is given in stage one then the cooling is given air cooling without the second stage.

First-Stage Graphitization. It was heated to temperatures of 850-900 ° C for ± 6 hours, held at a temperature of 900-970 ° C for 10 hours and decreased the temperature to 740 ° C quickly. The first stage of the nucleation formation of carbon tempering begins during heating towards the holding temperature and occurs very early during the holding time. During the containment phase, the existing carbide decreases from the iron structure, the splitting of the cerbide will begin to move. The length of holding time gives Graphite an opportunity to gather to other Graphites. When carbide is reduced, iron is rapidly cooled to 740 ° C first, to enter the second stage of Graphite formation.

On Stage Graphitization. slow cooling through extensive allotropic transformation of iron. During this process, simultaneously the free matrix Ferrite from pearlite and carbide is formed with a cooling speed of 2 to 28 ° C / h (3 to 50 ° F / h). This stage can not be carried out to form a perlitic microstructure [4] [5].

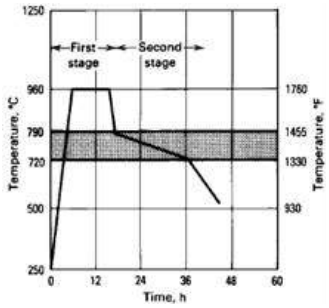

Figure 2 Diagram of annealing in forged cast iron [4]

2. METHODS

The research was carried out by the method as illustrated in the following flow chart:

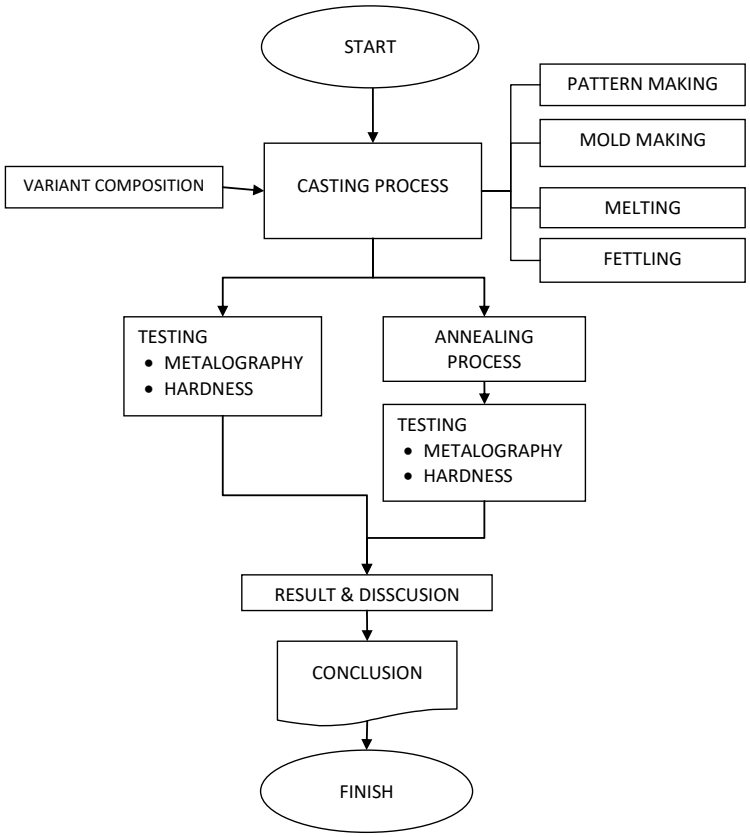

Figure 3: Flowchart of the Research Methods

The research activity was carried out by experimenting with making cast objects with triangular rods according to standards. Starting from designing variations of tellurium alloys, and designing and making patterns that will be used. Malleable cast iron materials are commonly used as pipes, or joints. The thickness of the pipe used is usually 12.5 mm, so the size of the test sample is in the form of a triangle with a base of 13 mm. The following is the size of the test sample shown in the image below.

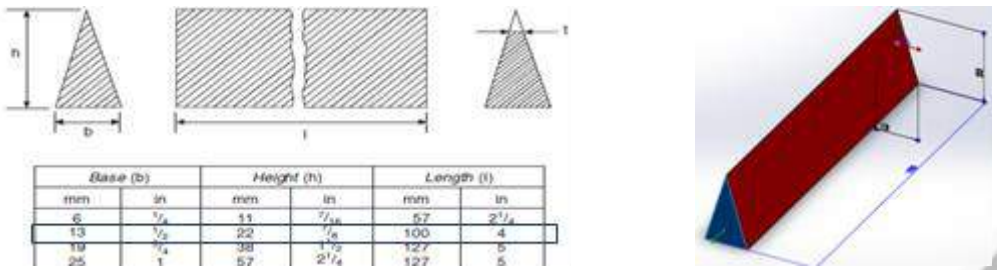

Figure 4 Test sample size (a) and Design of the test sample (b)

The size of the test sample was chosen from the size of the thickness. The test sample had the size of 13mm x 22mm x 100mm = 14300mm³ = 0.00143 dm³, using a specific gravity of 7.45, then weighing = 106.5grams.

The variable percentage of tellurium alloy is taken from the percentage of tellurium used in the CE meter. From the results of testing the composition, the value of 0.00144% is rounded up to 0.0015%. This value will be

used as a reference for the tellurium variable used. The following is a draft calculation of tellurium.

Table 1 Calculation of tellurium alloys

Nr.	Sample	Tellurium percentage	Tellurium Weight
1	Sample 1	0,0005%	0,0018 gram
2	Sample 2	0,001%	0,0036 gram
3	Sample 3	0,0015%	0,0054 gram
4	Sample 4	0,002%	0,0072 gram
5	Sample 5	0,0025%	0,0091 gram

After the test sample has been prepared, the next is the metal casting process. The metal is cast at a temperature of 1458^{o}C, with the alloy target composition as follows:

Table 2 Composition of ASTM A 220 [1]

Component Elements Properties	Metric
Carbon, C	2.0 - 2.9 %
Iron, Fe	95 %
Manganese, Mn	0.25 – 1.25 %
Phosporus, P	<= 0.05 %
Silicon, Si	1.0 – 1.75 %
Sulfur, S	0.030 –0.18 %

Figure 5 Casting process of samples in a mold (Tellurium powder is inserted into the mold before being cast)

The sample is prepared with an existing code, aligned with the test mat. 5 samples were inserted into the HT furnace. Increased from room temperature to 900 ºC within ± 6 hours, detained within 10 hours. The following is a graph of heat treatment performed [4].

Figure 6 Time-Temperatur curve of Annealing

At this stage, second-stage graphitization is not carried out to form the pearlite structure. The following is a picture of the stages of the heat treatment process carried out:

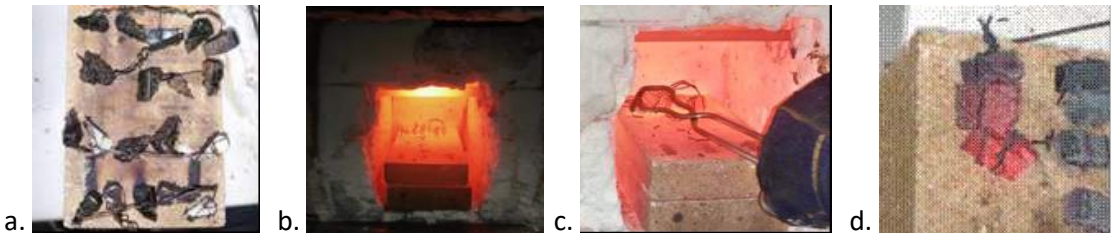

Figure 7 Preparation of test samples (a. Binding, b. Heating in the furnace, c. pulling out, d. cooling)

3. RESULTS AND DISCUSSION

Composition testing was carried out using the ORL brand ARL Spectrometry machine. From the composition testing performed, the following results are obtained:

Table 1. Reseacrh Subjects Characteristic Summary

Composition	Standard	Test Result
Carbon	2.00 – 2.90 %	2.80 %
Mangan	0.25 – 1.25 %	0.80 %
Silicon	1.00 – 1.75 %	1.34 %
Sulfur	0.03 – 0.18 %	0.03 %
Phospor	<= 0.05 %	0.02 %

In addition to composition testing using a spectrometry machine, samples were also tested for compositions using the EDS machine to detect tellurium. The following are the results of the SEM-EDS test:

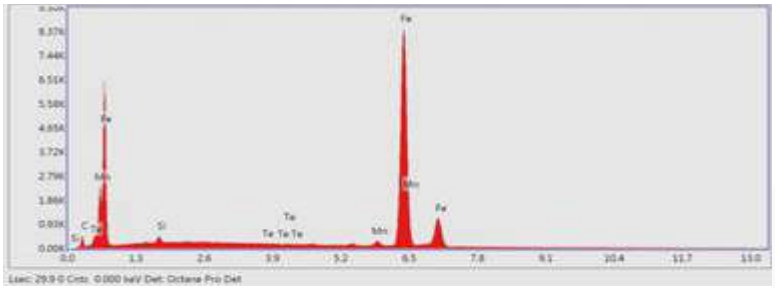

Figure 8 EDS test results

After the casting process, the analysis process is carried out from the test results. The following are the test results from each sample:

a.

Sample 1 (0,0005%)	
	Identifikasi : Warna patahan putih Jenis patahan getas
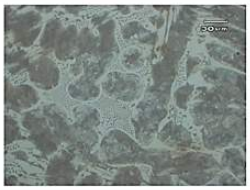	Identifikasi : Fasa yang terbentuk yaitu pearlit, ledeburit, dan karbida, dengan nilai kekerasan 61,9 HRC Gambar diambil dengan perbesaran 500x setelah dilakukan proses etsa nital 3%

b.

Sample 2 (0,001%)	
	Identifikasi : Warna patahan putih Jenis patahan getas
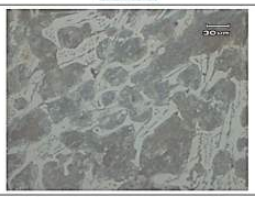	Fasa yang terbentuk yaitu pearlit, ledeburit, dan karbida, dengan nilai kekerasan 63,8 HRC Gambar diambil dengan perbesaran 500x setelah dilakukan proses etsa nital 3%

c.

Sample 3 (0,0015%)	
	Identifikasi : Warna patahan putih Jenis patahan getas
	Fasa yang terbentuk yaitu pearlit, ledeburit, dan karbida, dengan nilai kekerasan 64,7 HRC Gambar diambil dengan perbesaran 500x setelah dilakukan proses etsa nital 3%

d.

Sample 4 (0,002%)	
	Identifikasi : Warna patahan putih Jenis patahan getas
	Fasa yang terbentuk yaitu pearlit, ledeburit, dan karbida, dengan nilai kekerasan 65,3 HRC Gambar diambil dengan perbesaran 500x setelah dilakukan proses etsa nital 3%

e.

Sample 5 (0,0025%)	
	Identifikasi : Warna patahan putih Jenis patahan getas
	Fasa yang terbentuk yaitu pearlit, ledeburit, dan karbida, dengan nilai kekerasan 66,2 HRC Gambar diambil dengan perbesaran 500x setelah dilakukan proses etsa nital 3%

BEFORE HT (HRC)	
Sampel	Nilai kekerasan
1	61,9
2	63,8
3	64,7
4	65,3
5	66,2

Figure 9 Test results of samples as cast: cross section break surface and microstructure with 3% Nital etching: pearlite, ledeburit, and carbide:
a. sample no.1 (0,0005 Te), b. sample no.2 (0.001 Te), c. sample no.3 (0.0015 Te), d. sample no.4 (0.002 Te), e. sample no.5 (0.0025 Te)

After the heat treatment process, metallographic testing is carried out. In this process, graphite is taken from each sample. As for the testing position, it is in the middle of the sample. Next is the test area of each sample:

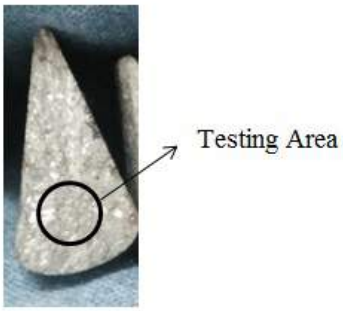

Figure 10 Metallographic testing area on the sample

The following is a non etching image from the Heat Treatment process. Images are taken with 200x magnification after the polishing process is done using alumina:

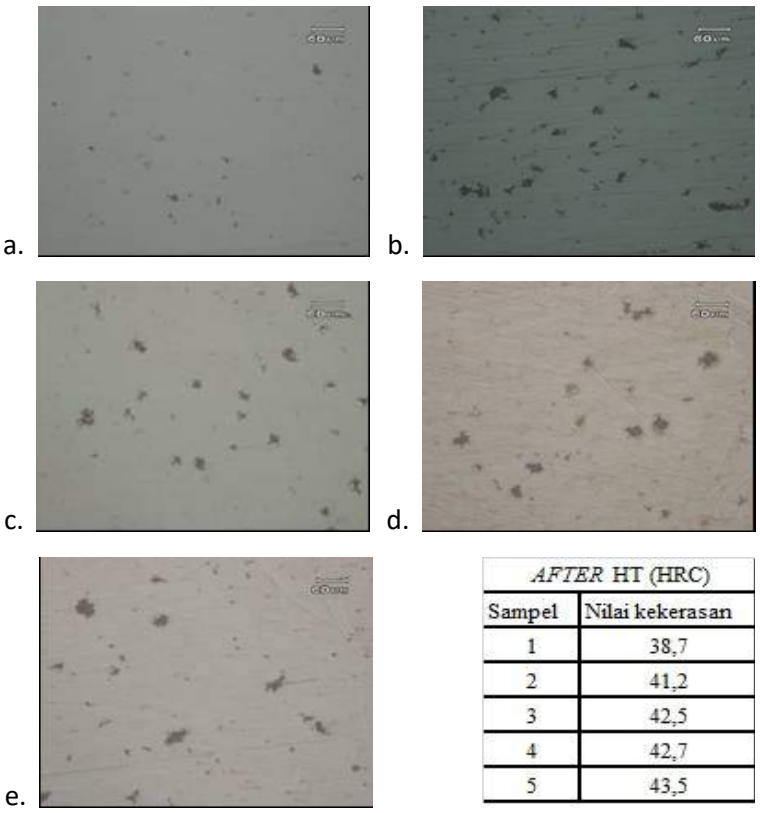

AFTER HT (HRC)	
Sampel	Nilai kekerasan
1	38,7
2	41,2
3	42,5
4	42,7
5	43,5

Figure 11 Samples 1 to 5 after heat treatment non etching 200x magnified:
a. Sample Nr. 1 (38.7 HRc.), b. Sample Nr. 2 (41 HRc.), c. Sample Nr. 2 (42.5 HRc.),
d. Sample Nr. 2 (42.7 HRc.), e. Sample Nr. 2 (43.5 HRc.)

From the test results, the analysis is obtained as follows:

1. All samples have the same microstructure phase, namely, ledeburit, pearlite, and cementite. And all samples have white faults. This means that before entering the treatment process, tellurium does not appear to affect the as cast material (seen from the phase type) at this stage.
2. Value of the phase hardness, there is an increase along with the addition of tellurium. The hardness testing area can be seen in the following picture:

Figure 12 Hardness Testing Area

3. After doing heat treatment, there is no difference in the results of the non-etching image, with a magnification of 500x. For more details, can be seen in the table below.

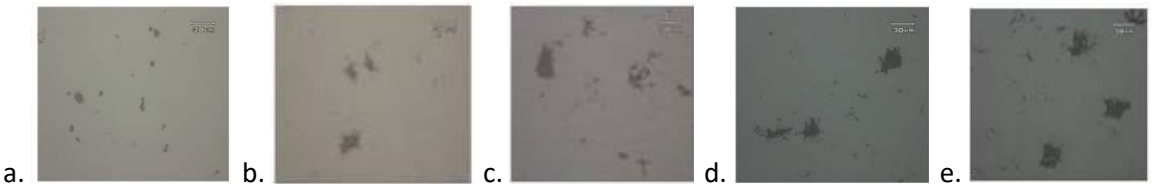

Figure 13 form of graphite sample 1 to 5 after annealling (graphite percentage):
a. Sample Nr. 1 (2%), b. Sample Nr. 2 (2.43%), c. Sample Nr. 3 (3.5%),
d. Sample Nr. 4 (3.6%), e. Sample Nr. 5 (6.5%)

4. Because the form of graphite does not look different, graphically the percentage of graphite is calculated. The results are as follows:

Table 4 Percentage value of graphite

Nr. Sample	Graphite Percentage
Sample 1	2 %
Sample 2	2.43 %
Sample 3	3.5 %
Sample 4	3.6 %
Sample 5	6.5 %

5. After the heat treatment process is carried out, the results show that tellurium has an influence on the size of graphite.

4. CONCLUSION

The results showed that all samples had white fault color or white cast iron with a structure before the heat treatment, ledeburit. After the heat treatment process is carried out, the results show that tellurium has an influence on the percentage of graphite in each sample. From the research that has been done, with the addition of tellurium the percentage of graphite becomes increased, from 2% to 6.5%. In addition, with the addition of tellurium, the value of material hardness has increased along with the percentage of tellurium added with a range of 38.7 HRC - 43.5 HRC.

From the research that has been done it can be concluded that tellurium has an influence on the form of graphite in malleable cast iron material.

5. REFERENCES

[1] American Standar Testing for Materials (ASTM), vol 03.01 E 10. *Standard Test Method for Brinell Hardness of Metallic Materials*. ASTM International, (2004).
[2] ASM Metal Handbook, vol 01. : *Properties and Selection Irons, Steels, and High-Performance Alloys*. ASM International, (1998).
[3] ASM Metals Handbook , vol 15: *Casting*. USA. ASM International, (1998).

[4] Brown, J. R., *Foseco Ferrous Foundryman' s Handbook*. Butterworth-Heinemann, (2000).
[5] E.G Mekhanicheva*, structure of malleable cast iron with tellurium*. Metal Science and Heat Treatment Vol. 17 issue 12 Metallurgy for engineers 4thedition,(1975).
[6] M.S. Soiński, D. Trepka, K. Lewandowski, *An attempt of assessing the production perspectives concerning malleable iron castings*, ISSN (1897-3310) Volume 9,Issue 3/2009, AFE, Poland, (2009).
[7] Semih Genculu, P.E., *Cast Irons; Properties & Applications*. Retrieved from https://pdhonline.com/courses/m568/m568_new.htm, (2015).
[8] Tuan Son Nguyen PhD, Kee Bong Yoon, *Failure of malleable cast iron sprinkler pipe end cap due to freezing of water within*, Department of Mechanical Engineering, Chung Ang University84 Heukseok-ro, Dongjak-gu, Seoul 06974, Korea. Retrieved from https://kundoc.com/pdf-failure-of-malleable-cast-iron-sprinkler-pipe-end-cap-due-to-freezing-of-water-w.html , (2016)

LOGIC
Journal of Engineering Design and Technology
Vol. 19 No.1 March 2019; p. 34 - 40

p-ISSN : 1412-114X
e-ISSN : 2580-5649
http://ojs.pnb.ac.id/index.php/LOGIC

GROUND FAULT PROTECTION USING OPEN BREAK DELTA GROUNDING TRANSFORMER IN UNGROUNDED SYSTEM

Supriyanto[1)], Hari Purnama[1)], dan Heri Budi Utomo[1)]

[1,2,3] Jurusan Teknik Elektro,
Politeknik Negeri Bandung,
Bandung, 40012

Correponding E-mail :
[1)] supriyanto_suhono@polban.ac.id
[2)] haripoernama@gmail.com
[3)] hbu@polban.ac.id

Abstract. One of the most common and difficult problems to solve in distribution power systems is the location and elimination of the ground fault. This paper presents a method for ground fault protection system scheme is used overvoltage relays and open break delta transformers, whereas for fault location detection using voltage transformers in star connections. An experimental for further understanding about the electrical distribution network, the ungrounded system will be operated at 20 kV on the primary and 380 V on the secondary. The model uses smaller nominal voltages consisting of 380 V on the primary and the secondary. The highest single line to ground fault value is used for consideration of ballast rating selection. The single line to lowest ground fault value is used for setting the threshold on the voltage relay (59N). The result of one phase fault protection mechanism works well at each point of interference, and voltage transformers are protected from overheating and damage. The lowest value of the single-phase to ground short circuit that occurs at the fault location at the farthest point of interference from the protection relay location is used for the threshold setting on the voltage relay. The one phase fault protection mechanism works well at each point of interference, and the voltage transformer is protected from overheating and damage..

Keywords :. ungrounding system, ground fault protection, open break delta transformers, overvoltage relay

1. INTRODUCTION

An ungrounding system is an earthing method that does not have a direct relationship between the star-point of a power transformer and the ground. Therefore, there is no circumference current of ground fault when the disturbance of the ground is occurring. The economic considerations and the maintained loading balance of the three-phases make this system selected.

Baldwin, T. shows a fault detection method in ungrounding and high impedance earthing systems using zero sequence current generator injections [1,2]. The technique developed is able to trace the disturbance to determine the location of the point of disturbance. Implementation of distribution network systems is using two methods. First, the installation of a zero-sequence signal generator was employed. When a ground disturbance is detected, the related relay initiates a signal generator to supply current through a system of looping back through the ground network after reaching the point of interference. The distance of electricity from the relay to the point of interference will be determined from the propagation of the signal generator. To avoid communication problems with other equipment, the frequency chosen for the signal generator is different from the frequency of the power line. The second, a remote ground-fault indicator (RGFI) was used. RGFI is connected to the zero sequence current of the transformer. When line-to-ground interference occurs, RGFI detects currents through a zero sequence and

then provides a physical indication of where the interference occurs. The test results from both methods were tested on ungrounding delta-connected networks and high-resistance grounding networks.

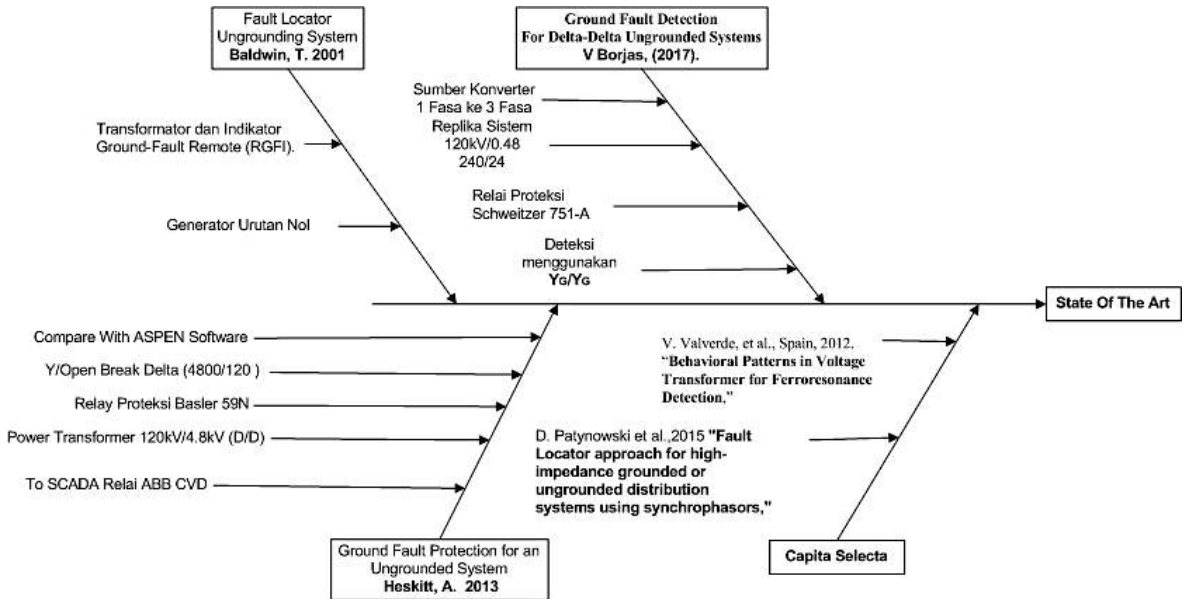

Figure 1. The state of the art of the simulator development

Further development is to study the effects of ferroresonance on ballast resistance which connected in parallel with overvoltage relays. For limiting the resonance between the VT inductance and the capacitance, the pattern system is developed referring to the technical experience. Most of the modern systems have a numerical relay in every phase, which can provide the necessary long-distance communication, but some utilities still use the solid state protection relay method.

Another method used is to determine the location of the fault by using a signal generator to zero sequence windings from the transformer. When a disturbance occurs, the relay starts generating a signal to send a current that will return through the soil network from the point of interference. This signal allows the relay to determine the distance between the points of interference from the relay so that the location of the fault can be specified in the system.

The ungrounding system has been studied extensively; A groundbreaking protection simulator design of an ungrounding system was developed by Heskitt [3] at the California Polytechnic State University in San Louis Obispo. On a network with a 120 kV/4.8 kV power transformer connected to Delta Delta, and a 4800 V/120 V voltage transformer, a 120 V secondary voltage connected by an open delta connected to the Basler-59N overvoltage protection relay. The two design simulators are replicas of the 12 kV electricity distribution system at the primary and 480 V at the secondary, which are reduced to 240 V at the primary and 24 V at the secondary. Current and voltage are connected to the Schweitzer 751-A protective relay which provides load monitoring and a ground fault detection scheme developed by V. Borjas [4] at Michigan Technology University USA.

In this study, we developed a design product for studying the soil disturbance protection in an ungrounding system of electric power distribution at a voltage of 20 kV on the primary and 380 V on a secondary, which was established at the Laboratory of Electric Power Distribution Systems, Bandung. In the simulator, the nominal voltage is simulated 380 V at primary and secondary. The ground disturbance protection system scheme uses an overvoltage relay (59N) and the voltage transformer on the primary with a star connection grounded, and the open secondary delta is grounded [5,6].

In this study, we will verify the consideration of choosing a ballast rating, and how to determine the overvoltage threshold setting, by the usage of four points of interference on the network. Therefore with the right selection, the protection against any location of interference along the network will be achieved, and the protection system elements are protected from damage. We will also look at the effect of short circuit interference in addition to a single phase to ground short circuit against the mechanism of the protection system.

2. METHODS

Functional Testing Design

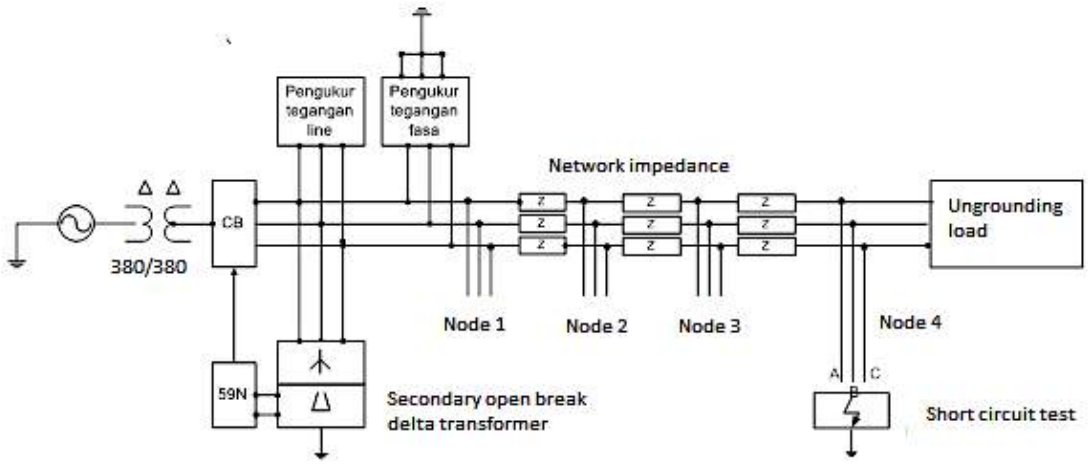

Figure 2. Functional testing design

The functional design that displays the relationship between function elements that become the framework in the simulator manufacturing process was shown in Figure 2. When one phase to ground interference occurs, the operating system will continue, in this condition cable insulation and equipment are under pressure. The effect that occurs during a zero voltage disturbance at the interrupted phase and the continuous phase voltage rises to √3 nominal voltage. The phase difference between the continuous stages drops from 120 degrees to 60 degrees. The testing process will run as follows:

1) Calculation and testing of one-phase to ground disturbances in the simulator will test for soil disturbances from four zones of disturbance point, 0% point of disturbance location as a representation of disturbance points at the substation, 25%, 50%, 75%, and 100% point location representation farthest interference.
2) The closest interference point (point 1) is used to determine the ballast capacity for the protection of a voltage transformer.
3) The farthest point of interference (point 4) is used to determine the overvoltage threshold set at a over voltage relay (59N).
4) Testing the mechanism of the one-phase to ground protection system of the four points of interference.
5) Examining the mechanism of the protection system against one phase to ground short circuit, phase to phase, two-phase to the ground, and three phase short circuit

Voltage During One Phase Disruption to the Ground

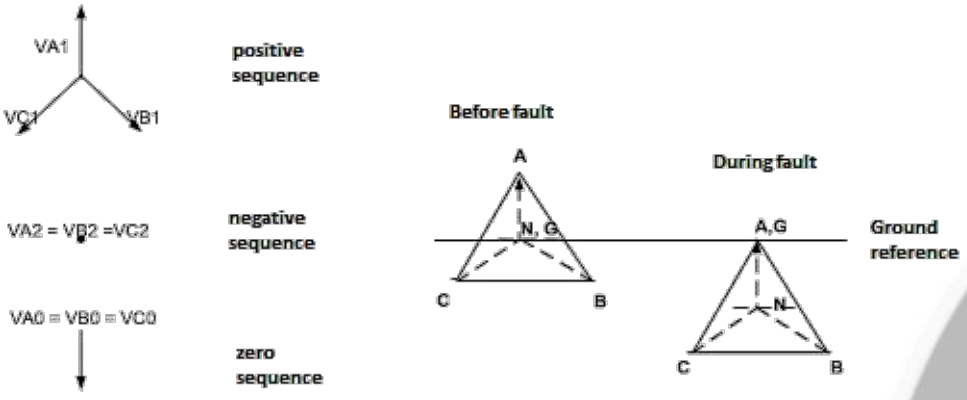

Figure 3. Ground Disturbance on Floating Grounding Systems

Protection for ground fault mechanism and voltage threshold settings

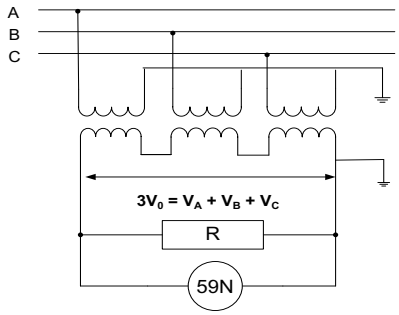

Figure 4. Open Break Delta Network and Overvoltage Relay (59N)

The concept of protection of zero sequence voltage characteristics in a not grounded system when a single phase fault occurs to the ground is shown in Figure 4. Voltage transformers in an open break delta relationship will give an increasing voltage signal in the event of a ground disturbance. The overvoltage protection relay ground disturbance will detect ground faults and give Circuit Breaker commands to break up [7,8].

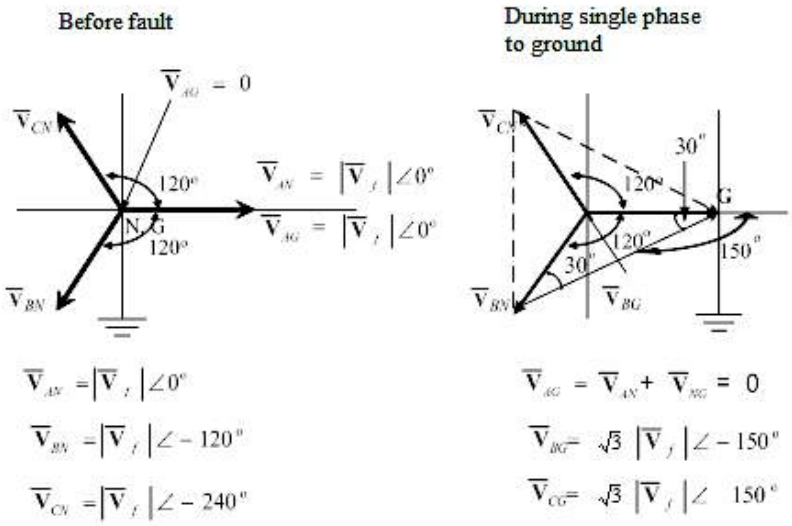

Figure 5 Vector Chart of The Open Break Delta Terminal Exit Voltage

When a ground fault occurs, the voltage will rise three times the phase voltage to nominal neutral. This voltage will be detected in the open break delta transformer terminal.

3. RESULTS AND DISCUSSION

Table 1. Results of Calculation of Interference Voltage One Phase to Ground Short Circuit

Type of fault	Voltage A V_A(Volt)	Voltage A V_B(Volt)	Voltage A V_C(Volt)	Voltage 59N V_0(Volt)
Before a fault in node 1	$220\angle 0^0$	$220\angle -120^0$	$220\angle 120^0$	0
Before a fault in node 2	$214\angle 0^0$	$214\angle -120^0$	$214\angle 120^0$	0
Before a fault in node 3	$208\angle 0^0$	$208\angle -120^0$	$208\angle 120^0$	0
Before a fault in node 4	$202\angle 0^0$	$202\angle -120^0$	$202\angle 120^0$	0
During ground fault in 1	0	$380\angle -150^0$	$380\angle 150^0$	$144\angle 180^0$
During ground fault in 2	0	$370\angle -150^0$	$370\angle 150^0$	$140\angle 180^0$
During ground fault in 3	0	$360\angle -150^0$	$360\angle 150^0$	$136\angle 180^0$
During ground fault in 4	0	$350\angle -150^0$	$350\angle 150^0$	$132\angle 180^0$

The purpose of the installation of detainees is to protect the transformer from working according to the rating of its capacity. From table 1 we get the highest relay voltage of 144 volts. The secondary rating of the ballast rating is determined by the capacity (VA) per phase of the voltage transformer divided by the secondary voltage transformer per phase rating. Therefore, for a 50 VA voltage transformer with a secondary voltage of 48 volts, the secondary current rating is 50/48 = 1 ampere. Ballast resistance is the voltage on the terminal relay 144 volts, the ballast resistance required is 144/1 = 144 ohms while the minimum resistor power is 144 x 1 = 144. In the simulator selected R = 200 ohms, and 150-watt ballast power.

Overvoltage settings 59N [5], from Table 1 shows that the value of the relay terminal voltage when a one-phase short circuit occurs at the lowest ground is 132 volts. The relay threshold voltage is set at 120 volts, and the disconnection time setting with inverse characteristics uses TDS = 40. The protection system is needed for short circuit ground fault until the breaker works clearing the interference and separating the part that is experiencing ground disturbance with a 10 second break time. IEEE Std 32-1972 [9,10,11].

Test Protection Performance in Various Short-circuit Interferences

When one phase to ground interference occurs, the operating system will continue, in this condition cable insulation and equipment are under pressure. The effect that occurs during a zero voltage disturbance at the interrupted phase and the continuous phase voltage rises to √3 nominal voltage. The phase difference between the undisturbed phases drops from 120 degrees to 60 degrees. When a ground fault occurs, the voltage will increase three times the phase voltage to nominal neutral. This voltage will be detected in the open break delta transformer terminal.

Table 2. The Measurement Results of Short-circuit Voltage Disturbance Furthest Point*

Type of fault	Voltage A V_A(Volt)	Voltage A V_B(Volt)	Voltage A V_C(Volt)	Voltage 59N V_0(Volt)
Before a fault	202	202	202	0
Single phase to ground faults	0	350	350	132
Phase to phase faults	202	101	101	0
Two phase to ground faults	303	0	0	66
Three phase faults	0	0	0	0

*) Determined at VT ratio 220/48, based on voltage measurement on the disturbance point

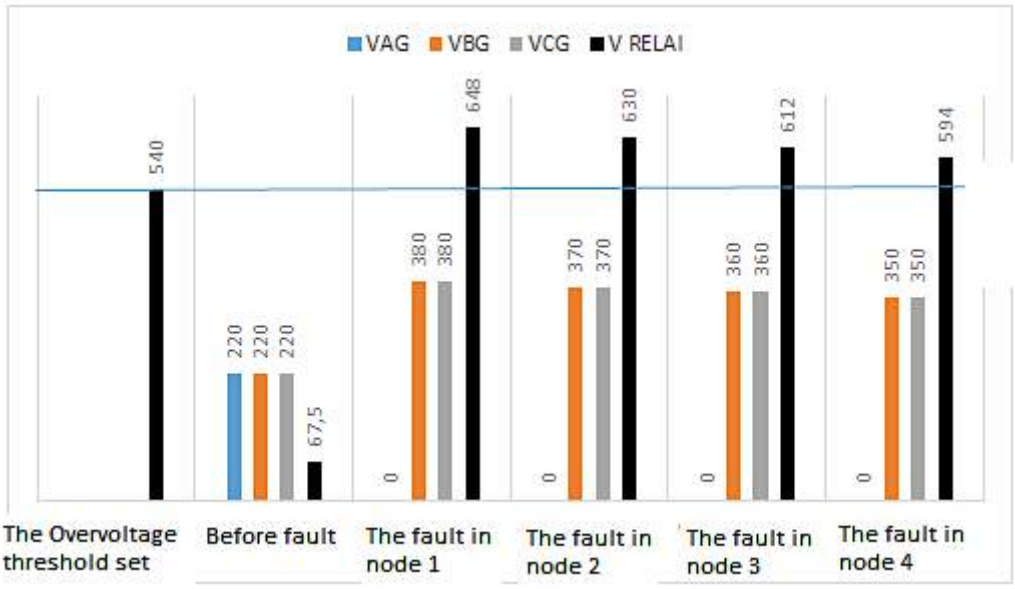

Figure 6 The Voltage at Single-Phase to Ground Fault in Function of Disturbance Location

From the graph in Figure 6 shows that the setting based on relay voltage at point 4 can protect all four points of interference. Using the characteristics of the inverse time function voltage with a 120-volt setting, and TDS = 40. In Figure 7 it is shown that in interruptions at point 4; 3; 2; 1 with a sequential termination time of 3.5 seconds; 3 seconds; 2 seconds, 1 second.

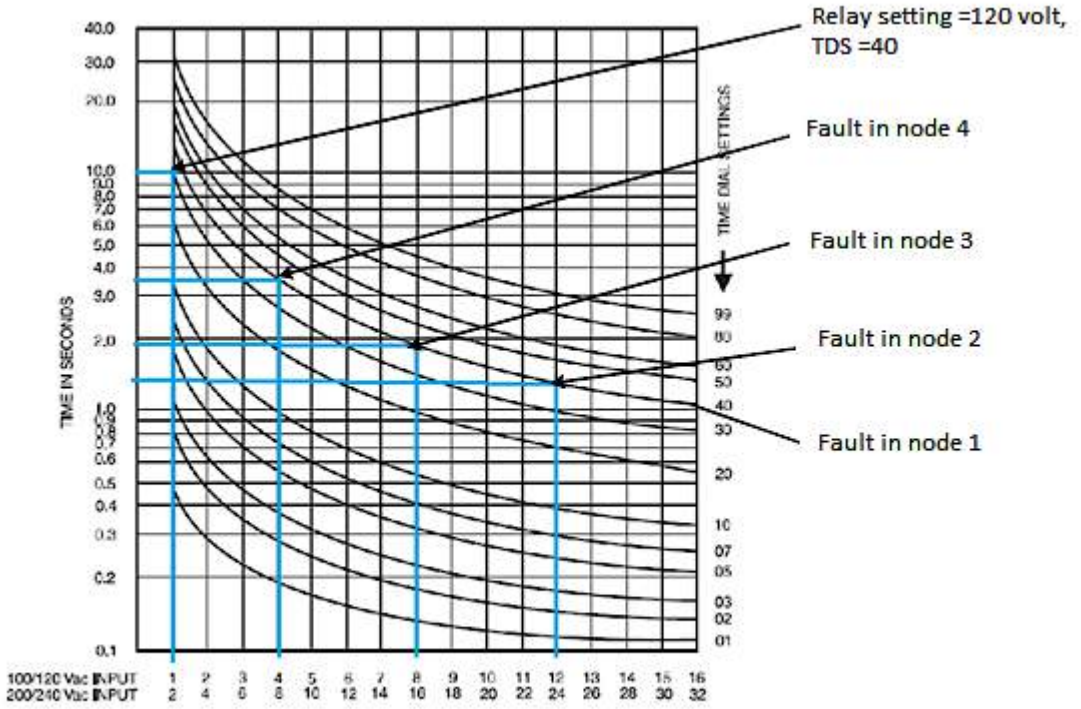

Figure 7 The Characteristic of The Overvoltage in Time of Inverse Termination

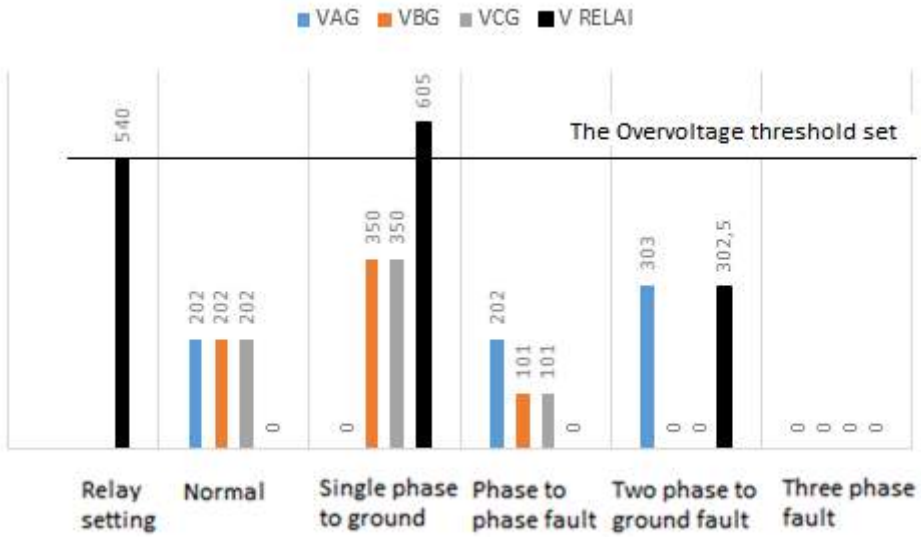

Figure 8 Voltage Function of Different Types of Disturbance

The results of testing with various types of short circuit interference indicate that this protection system only protects against one phase voltage to the ground. From this test, it can be seen that overcurrent protection of phase disturbances is still needed to provide phase disturbance protection.

4. CONCLUSION

The highest one-phase short-to-ground value is the location of the disturbance that occurs at the closest location to the installed relay used for consideration of ballast rating selection. The lowest value of the single-phase to ground short circuit that occurs at the fault location at the farthest point of interference from the protection relay location is used for the threshold setting on the voltage relay. Referring to the calculation results of the highest one-phase voltage at point 1 is 144∠180° volts, and the lowest is at point 4 of 132∠180° volts. 200-ohm ballast impedance with a power capacity of 150 watts, and an overvoltage threshold setting of 120 volts with a TDS of

40. The one phase fault protection mechanism works well at each point of interference, and the voltage transformer is protected from overheating and damage.

Testing with other short-circuit parameters in addition to the short circuit of one ground phase is not able to initiate the circuit breaker to operate, only in a single phase short circuit to the ground that the protection relay works to decide the network breaker. Therefore phase short circuit security is still needed to protect the network

5. REFERENCES

[1] Baldwin, T., F. Renovich, L. Saunders. 2001. "Fault Locating in Ungrounded and High-Resistance Grounded Systems," *IEEE Trans. Ind. Appl.,* vol. 37, no. 4, pp. 548-553, July/Aug 2001.

[2] J. Roberts, H.J. Altuve, and D. Hou. 2001. "Review of ground fault protection methods for grounded, ungrounded and compensated distribution systems," Proceedings from Conference: at the 28th Annual Western Protective Relay, Washington, October 23-25, 2001. [Online]. Available: http://www.selinc.com/techpprs/6123.pdf

[3] Heskitt, A. and Mitchell, H. 2013. Ground Fault Protection for an Ungrounded System. [online] available: http://www.ece.mtu.edu/faculty/bamork/ EE5223/EE5223TermProj_Ex3.pdf, accessed on 10 Maret 2018.

[4] V. Borjas, Daniela. 2017. "Ground Fault Detection For Delta-Delta Ungrounded Systems," Electrical Engineering Department, California Polytechnic State University-San Louis Obispo, 2017. [online] available: http://digitalcommons.calpoly.edu/cgi/ viewcontent.cgi?article=1433&context=eesp accessed on 4 April 2018

[5] Basler. 2013. *The 59N and Broken Delta Applications,* Basler Electric Co., Highland.

[6] Supriyanto. 2011. Rancang Bangun Modul Praktikum Sistem Proteksi Jaringan Distribusi Tegangan Menengah Menggunakan Rele Arus Lebih Type MCGG 52 *Jurnal Ilmiah TEDC*, Mei 2011, Vol: 5, No.1, Tahun 2011, ISSN: 1978-0060.

[7] V. Valverde. 2012"Behavioral Patterns in Voltage Transformer for Ferroresonance Detection," Elec. Eng. Dept., E.T.S.I.I, Univ. of Basque Country, Bilbao, Spain, 2012.

[8] Yudi P.H., Supriyanto. 2011. Perancangan Alat Sinkronisasi Integrasi dengan Sistem Proteksi untuk Interkoneksi Pembangkit Skala Kecil., *Jurnal Ilmiah TEDC*, Mei 2011, Vol:5, No.: 2, Tahun : 2010, ISSN : 1978-0060.

[9] V. Dusang. 2008. A Ground Fault Protection Method for Ungrounded Systems, Proceedings from IEEE Conference 2008: *Electrical Power & Energy Conference, pp. 1-6, 2008.*

[10] M. Shen. 2008. Grounding Transformer Application, Modeling, and Simulation, Member, IEEE, L. Ingratta, and G. Roberts, Proceedings from IEEE Conference 2008: *Power and Energy Society General Meeting - Conversion and Delivery of Electrical Energy in the 21st Century, 2008 IEEE*

[11] W. Piasecki. 2007. "Mitigating Ferroresonance in Voltage Transformers in Ungrounded MV Networks," IEEE Trans. Power Del., vol. 22, no. 4, pp. 2362-2369, Oct 2007.

LOGIC
Journal of Engineering Design and Technology
Vol. 19 No.1 March 2019 ; p. 41 - 46

p-ISSN : 1412-114X
e-ISSN : 2580-5649
http://ojs.pnb.ac.id/index.php/LOGIC

DESIGN AND DEVELOPMENT OF LOGIN SECURITY SYSTEM USING RADIO FREQUENCY IDENTIFICATION

I Gede Sujana Eka Putra [1], Ni Luh Putu Labasariyani [2]

1,2) Informatic Engineering Department, STMIK STIKOM Indonesia

Jl Tukad Pakerisan 97 Denpasar Bali Indonesia

Phone :+62-361-256995

Correponding email
[1] sujanaekaputra@stiki-indonesia.ac.id
[2] labasariyani@gmail.com

Abstract. *System security is important in information systems to prevent unauthorized users from accessing data. Login system applies security using encrypted passwords stored on RFID cards. This research designed login security system storing encrypted password using MD5 encryption into the Mifare Tag RFID card and equipped NFC reader to read data from RFID Card. By storing encrypted password characters on RFID cards, login system security is stronger and cannot be traced by unauthorized parties to log into systems. Some stage of system design are through study of literature, designing process flow, system algorithms, designing encryption methods and system interfaces, writing card module coding, card reading module coding, implementation, and system testing. The system login applied by scanning RFID card on the NFC reader, if the password on RFID matches then the user successfully logs into the system. Based on the testing of RFID Tag readings, the maximum distance from the reading of RFID Tag cards is up to 7 cm with a reading range of 0^0 to 30^0 with a success rate of 100% authentication. By using RFID Tag cards, increase security for logging into the system, because user cannot log in without having a card with the appropriate password.*

Keywords : System Login, RFID Card, Encryption, Security, Password.

1. INTRODUCTION

System security and data confidentiality are important in information systems to prevent unauthorized users from accessing data. RFID (radio frequency identification) is a technology that combines the function of electromagnetic or electrostatic coupling in the radio frequency portion of the electromagnetic spectrum, to identify an object [1]. RFID is used as a tool to automatically control a chain of activities [2].

Previous research has implemented RFID in the patient's medical record queue system, aimed at reducing patient queuing time when processing medical records at outpatient registration in hospitals, where RFID is used for patient's unique code. This unique code will automatically display patient data so that it does not require search time for patient files that can increase the patient queue time [3].

System logins as system access security are implemented through inputting passwords, where passwords are privacy and confidential. The current condition of using a login password is registered through the username and password data input on the system. Although the password has been encrypted but because it is manually inputted into the system, it is possible that the password can be tracked with a certain algorithm so that unauthorized users can track and successfully enter the information system. A risk will appear if the password entered during the system login is not encrypted or made with words that are easily guessed by other users. This is an opportunity for sniffers to track the password to log into the system. Cryptography aims to provide security services, including security to maintain passwords. The character of the password that is owned must be

confidential so that the character password cannot be traced by people who are not entitled or who have no interest. In terms of system access security, it is important to pay attention to security by encrypting the password on the login system before the data is sent to the server [4].

The use of RFID (radio frequency identification) replaces the 1-dimensional and 2-dimensional barcode system (quick response code) which is generally still widely used RFID (Radio Frequency Identification) as one of the flexible, easy to use and very suitable identification technology for automatic operation. RFID is a card (card) that can only be read (read only) or can be read and written (read / write), does not require direct contact or light paths to operate, can function in a variety of environmental conditions, and provide a level of data integrity high, and difficult to fake, so RFID can provide a high level of security [5]. This digital transaction system using RFID is more profitable compared to conventional transaction systems both in terms of effectiveness and security. The advantage is that it only requires one card to access all digital transaction data compared to the current one which requires a lot of cards to access it. With one RFID card this can make it easier for humans to access various digital data transactions [6]. RFID can carry out automatic controls in various fields such as retail, manufacturing, library, supply chain and medical applications that have applied RFID technology [3]. RFID implements electromagnetic sensors that read tags through certain frequencies. Other research related to sensors is implementing motion sensors, temperature sensors and sound sensors to automatically turn on the lights on the toilet and turn off the lights automatically when no one is in the toilet [7]. The research conducted is designing a login system security by storing encrypted password characters into radio frequency ID (RFID), using RFID cards and NFC devices to read data on RFID cards. Password characters are encrypted using the MD5 encryption method. By storing encrypted password characters on RFID cards, login system security is stronger and cannot be traced by unauthorized parties to log into information systems. The system login is done through scanning RFID cards on NFC devices, if the password on RFID is correct, then the user can log in to the system, otherwise cannot enter the system. There are three types of labels on RFID [8,9], namely 1) active RFID labels require a power source in the production process so that they are larger in size, and emit signals to label readers and are usually more accurate than passive RFID labels. Active RFID labels have strong signals that can be used in environments that are difficult to reach such as water, or long distances to transmit data. 2)Passive RFID label itself does not use internal electricity and relies on the RFID reader in sending data. Passive RFID labels are more suitable for use in warehousing environments where there is rarely interference and relatively short distances, because passive RFID labels do not use internal resources so passive RFID labels are smaller and cheaper to produce. 3). Semi-Passive RFID label resembles an active RFID label where the Semi Passive RFID label has internal resources but does not emit a signal to the RFID reader.

Based on the above description of the background, the issues to be raised in this research are as follows: (a) How to design login security system by using radio frequency identification stages ?, (b) How the maximum distance of reading RFID Card into NFC Card reader?. The purpose of this study are as follows: (a) to determine the stages required for design and development login security system by using radio frequency identification stages, (b) to determine maximym distance of reading RFID Card into NFC Card. The benefits of this research are as follows: (a) to complete the project on time so that its budget use becomes efficient, and (b) To apply the new technology gained related to identify unique code by implementing RFID Card. The limitations of the research problems are: (a) research was design and development application for login using RFID Card, MIFARE Card, and (b) password character stored in RFID Card with encrypted to MD5 algorithm.

2. METHODS

2.1 Flow Chart

The research phase consists of several stages: library research, designing process flow and login system algorithms, designing encryption methods and system interfaces, writing program code to write and read password characters to RFID cards, system implementation and system testing.

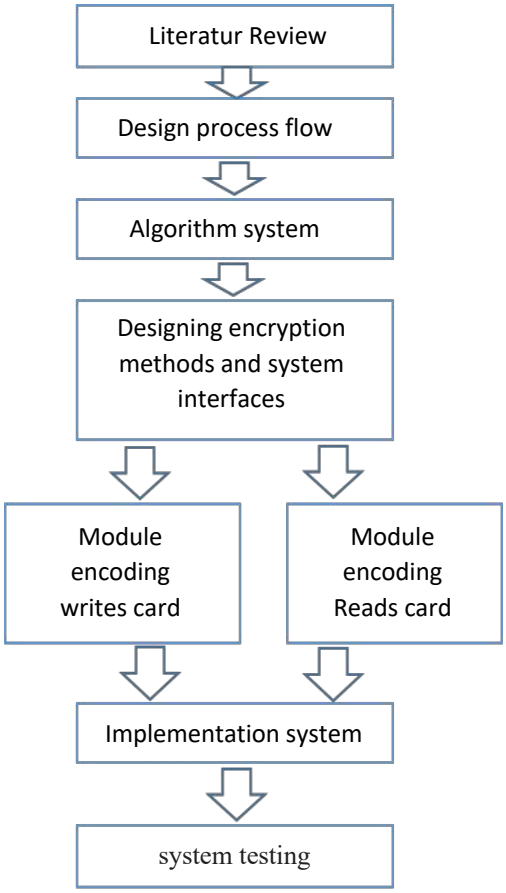

Figure 1. The Flow Chart of System Design and Development.

2.2 The Time of System Design and Development
The research execution time is 10 weeks.
2.3 Research Location
For the location of this research, it was taken in STMIK STIKOM Indonesia

3. RESULTS AND DISCUSSION

3.1 User Interface Screen Display
Main Menu User Interface as Figure 2 follow:

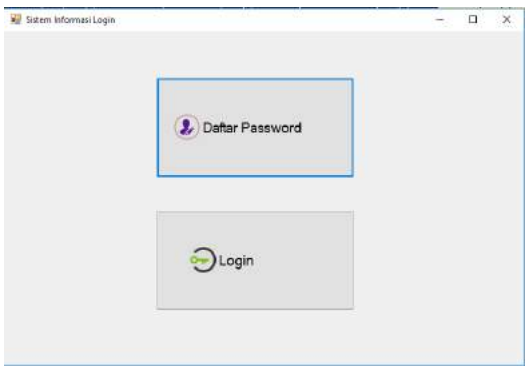

Figure 2. Main Menu User Interface

The main menu module consists of 2 parts, namely a list of passwords and logins. Register a password to register passwords and save passwords on the RFID card while the login functions to enter the system through RFID card scanning.

Figure 3. Password Registration Module

The password registration module functions to register passwords, encrypt these passwords and store passwords in the database and into the RFID card so that in the RFID card there is an encrypted password. In password registration, applying validation, the character password must consist of a combination of capital letters, numbers and symbols. The password character must be the same as the character in rewriting the password. The maximum number of password characters is 12 characters. The password validation display is as follows.

a. Display a combination of numbers, letters and characters.

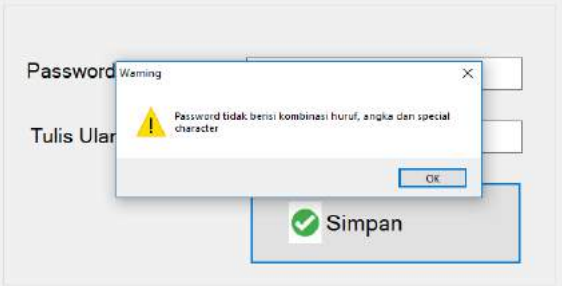

Figure 4. Validation of combination password letter, alphabet and character

b. Password validation maximum 12 character

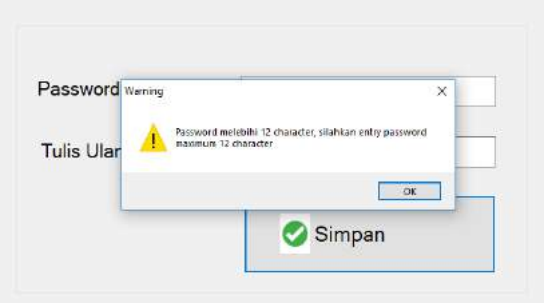

Figure 5. Password Validation maximum 12 character

c. Display password successfully saved in NFC Card

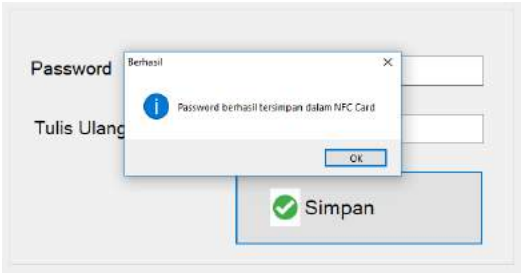

Figure 6. *Password* successfully stored in *NFC Card*.

Passwords that have been registered in the system are stored in the database in the form of data encryption, making it difficult to detect the character of the password used and increase security for logging into the system.

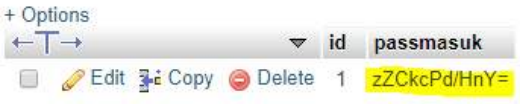

Figure 7. Encryption *password* result using MD5 algorithm

Figure 8. *Scanning RFID Module*

The RFID scanning module serves to scan RFID cards to read passwords on the card, then authentication and verification of the password is done to enter the information system.

Figure 9. Information System Login User Interface

This module is the main menu module after the user has entered the system after verifying the password of the RFID card that was scanned on the NFC Reader scanning tool.

Testing Distance Between *Tag* and *NFC Reader* and Testing Result Angle *Tag* Relative to *NFC Reader* as Table 1 and Table 2 follows.

Table 1. Testing Distance Between *Tag* and *NFC Reader*

Tag Distance relative to *NFC Reader*	Frequency		
	Test1	Test2	Test3
1 cm	√	√	√
2 cm	√	√	√
3 cm	√	√	√
4 cm	√	√	√
5 cm	√	√	√
6 cm	√	√	√
7 cm	√	√	√
8 cm	-	-	-

Table 2. Testing Result Angle *Tag* Relative to *NFC Reader*

Angle Tag relative to NFC Reader	Frequency		
	Test1	Test2	Test3
5^0	√	√	√
10^0	√	√	√
15^0	√	√	√
20^0	√	√	√
25^0	√	√	√
30^0	√	√	√
35^0	-	-	-

4. CONCLUSION

The conclusion of this research is that the system design stages consist of literature studies, designing process flow, designing system algorithms, designing encryption methods and system interfaces, writing card module coding, card reading module coding, system implementation, and system testing. Testing the system by scanning an NFC Card Tag (RFID) card on a card reader, obtained the results of testing the maximum distance from the reading of the NFC Tag card is up to 7 cm with the reading angle range 0^0 until 30^0 with the success rate of the authentication process at 100%. By using an NFC card, increase security for logging into the system, because it is difficult to log in without having a card with the appropriate password.

5. REFERENCES

[1] Julian Onibala. 2015. Perancangan Radio Frequency Identification (RFID) Untuk Sistem Absensi Berbasis Mikrokontroller ATmega 8535" E-Journal Teknik Elektro dan Komputer vol.5 No. 7, ISSN: 2301-8402, pp. 45 – 49.

[2] Charles P M Siahaan. 2014. Perancangan Sistem Pembayaran Parkir Secara Otomatis Menggunakan RFID (Radio Frequency Identification"). Jurnal Singunda Ensikom Universitas Sumatera Utara (USU), Vol. 9 No. 3, Desember 2014.

[3] Musfirah Putri Lukman. 2018. Implementasi Teknologi RFID Pada Sistem Antrian Rekam Medis Pasien Di Rumah Sakit. Jurnal Ilmiah Ilmu Komputer, Vol.10 No.1, April 2018.

[4] Dyna Marisa Khairina. 2011. Analisis Keamanan Sistem Login", Jurnal Ilmiah Ilmu Komputer, Vol.6 No.2.

[5] Joseph Dedy Irawan. 2017. Pengembangan Kunci Elektronik Menggunakan RFID dengan Sistem IOT". Jurnal Industri Inovatif, Vol. 6, No.2, p. 28 -32, September 2017.

[6] Ferdo Eko Christanto. 2017. Implementasi Kartu RFID Untuk Sistem Transaksi Basis Data Digital", Jurnal Teknologi Rekayasa, Vol.22, No.3, Desember 2017.

[7] Musfirah Putri Lukman. 2018. Sistem Lampu Otomatis Dengan Sensor Gerak, Sensor Suhu dan Sensor Suara Berbasis Mikrokontroller", Jurnal Resistor. Vol.1 No.2, Oktober 2018.

[8] Noname. 2019. Advanced Card Systems Ltd. "ACR122U USB NFC Reader. Available at: https://www.acs.com.hk/en/products/3/acr122u-usb-nfc-reader/, 2019 [accessed: January 31, 2019].

[9] Wenny Marthiana. 2018. Suatu Kajian Literatur Aplikasi Radio Frequency Identification dalam Bidang Pertanian. Jurnal Inovasi Vokasional dan Teknologi, Vol.18, No.1, 2018.

LOGIC
Journal of Engineering Design and Technology
Vol. 19 No.1 March 2019; p. 47-53

p-ISSN : 1412-114X
e-ISSN : 2580-5649
http://ojs.pnb.ac.id/index.php/LOGIC

SONGKET INDUSTRY WASTEWATER PROCESSING USING ELECTROCOAGULATION METHOD

Rusdianasari[1)], Ibnu Hajar[1)], dan Indri Ariyanti[2)]

1,2) Chemical Engineering Department, Politeknik Negeri Sriwijaya,
3) Informatic Management Department, Politeknik Negeri Sriwijaya

Srijaya Negara street, Palembang, 30139

Correponding email 1) : rusdianasari19@gmail.com

Abstract. The increment of Songket popularity as the traditional fabric from South Sumatra increases the production of Songket and the wastewater produced during the dying process. The dying process produces the reddish wastewater, and if it is disposed of directly into the environment, it will have a negative impact on the waters. The wastewater treatment of this reddish liquid is by electrocoagulation method. Electrocoagulation method is contaminants removal by electrical and chemical treatment system. The electrocoagulation method in this research was conducted in a batch where the wastewater was treated using 16.5 x 7.0 x 0.2 cm aluminum electrode. The parameters varied were the current density and processing time to determine the pH value, color intensity, BOD5, COD, TSS, and phenol levels. The optimum condition obtained from this study at a current density of 25 A/m^2 with a processing time of 160 minutes. The effectiveness of Songket wastewater electrocoagulation was 67.28% for TSS, 54.13% for BOD5, 63.64% for COD, color intensity 79.21% and phenol content of 74.93% respectively. The result has fulfilled the quality standard of textile industry wastewater treatment.

Keywords : wastewater, songket industry, electrocoagulation, aluminum electrodes.

1. INTRODUCTION

The liquid waste of the songket industry has become a major problem in controlling the environmental impact of the textile industry. The entry of dyes from waste into the waters has caused the physical and chemical characters of water resources to change. In order to fulfill quality standards, liquid waste must be processed in an integrated manner, both those produced during the production process and after the production process [1].

The management of liquid waste in the production process is intended to minimize the volume, concentration, and toxicity of waste. Processing of liquid waste after the production process is intended to eliminate or reduce the levels of pollutants contained in it, until liquid waste meets the requirements to be disposed of (fulfilled the quality standard) [2].

The most liquid waste management carried out by textile factories is coagulation (clumping) followed by adsorption of pollutants by passing wastewater through zeolite and activated charcoal [3].

There are several centers of songket fabric industry in Palembang that can be found in Ilir Barat II District and 14 Ulu Village. Every songket fabric production is preceded by yarn dyeing activities. Each dyeing process will produce 40 liters/day of waste flow for one limar set for one type of color while the colors used vary. There are 83 units of yarn dyeing business units, so in a month 1200 liters of wastewater is produced or 438,000 liters/year for one type of color. If the color used consists of 5 kinds of color, 2.190,000 liters/year of liquid waste will be produced. Almost all other songket industries are home industries that are not equipped with adequate wastewater treatment [4,5].

To overcome the problem of songket industrial waste above, it requires an innovative, inexpensive and effective method of processing waste before the liquid waste is disposed of into the environment [6]. The electrocoagulation method can be used to treat songket industry wastewater and has several advantages compared to the coagulation method using chemicals [7],

Electrocoagulation is the process of clumping and deposition of fine particles contained in water using electrical energy. The electrocoagulation process is carried out on an electrolytic vessel in which there are two direct current electric conductors that we know as electrodes. The part of the electrode immersed in the waste solution will be used as an electrolyte [8]. If in one electrolyte solution two electrodes are placed then the electrode is flowed by a direct current of electricity then an electrochemical process will occur in the form of electrolyte decomposition symptoms, i.e., positive ions (cations) move to the cathode and receive electrons reduced and negative ions move to the anode and give up the oxidized electron, so that later it will form a floc which is able to bind contaminants and particles in the waste [9].

The electrocoagulation process is formed by dissolving metal from the anode which then interacts simultaneously with hydroxy ion and hydrogen gas produced from the cathode [10]. Matteson introduced "Electronic Coagulator" where the electric current given to the anode dissolves aluminum into a solution which then reacts with hydroxy ions (from the cathode) to form aluminum hydroxy [11]. Hydroxy flocculates and coagulates suspended particles so that a process of separation of solids from wastewater occurs. A similar process was also carried out in Brittain in 1956, only the anode used was iron and used to treat river water [11].

2. METHOD

For wastewater treatment, a series of electrocoagulation devices are used consisting of aluminum electrodes, regulators, digital multimeters, and anode and cathode connecting cables. The sample used was liquid songket industry wastewater in the Kertapati area. The stages of songket industry wastewater treatment are:

a. The electrodes used were 16.5 cm long, 7 cm wide, 1 cm distance between electrodes, 0.2 cm electrode thickness.
b. Songket liquid waste is inserted as much as 800 mL into a 1000 ml beaker.
c. After the beaker is filled with waste, the voltage flow is turned on by activating the adapter using a 12 volt voltage with variations in current density of 25 A/m^2, 45 A/m^2, 65 Am^2, and 85 A/m^2 and the operating time of each process for 40 minutes, 80 minutes, 120 minutes, and 160 minutes.
d. The results of the electrocoagulation process were deposited for 2 hours
e. Next, the distillation from the precipitate is filtered.
f. The characteristics of the electrocoagulation process were determined by measuring pH, BOD5, COD, TSS, color intensity, and phenol levels in the filtered surface.

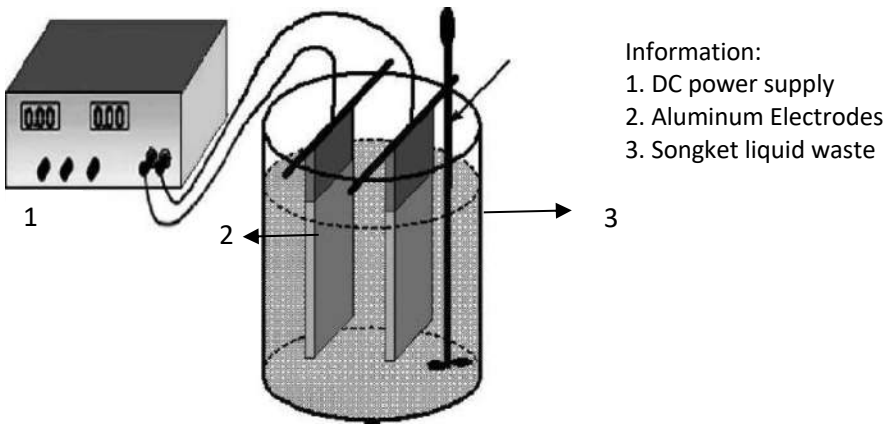

Figure 1. Electrocoagulation Reactor

3. RESULTS AND DISCUSSION

Preliminary Analysis of Characteristics of Songket Liquid Waste

Results of Preliminary Analysis of Songket Liquid Waste as Table 1.

Table 1. Results of Preliminary Analysis of Songket Liquid Waste

No.	Type of Analysis	Quality standards	Analysis results
1.	pH	6 – 9	10.73
2.	BOD_5 (mg/L)	50	213.5
3.	COD (mg/L)	100	702
4.	TSS (mg/L)	200	985
5.	Color intensity	-	1120
6.	Phenol levels (mg/L)	0.5	7.85

Source: Environmental Quality Standards based on South Sumatra Governor Regulation No. 8, year: 2012.

From the results of the initial analysis of songket liquid waste in Table 1, the pH value and the decrease in TSS, BOD5, COD, color intensity, phenol levels did not exceed the clean water quality standard. However, high BOD5 and COD values must be processed to reduce BOD5 and COD levels. This is because the high levels of BOD5 and COD will cause potential contamination for both surface water and groundwater. In addition, the level of phenol in songket liquid waste also exceeds the limit of the quality standard of clean water needs to be reduced in order to be able to meet the requirements for disposal to the environment, and those that have reached or less than the standard quality of phenol can be disposed of into the environment. Clean water is water that meets the requirements for the environment, both from pH, BOD5, COD, TSS, color intensity and phenol levels.

Effect of Current Density and Process Time on pH

The pH level is an expression of the concentration of hydrogen ions (H^+) in water. pH is very important as a parameter of clean water quality because pH controls the type and speed of reaction of some materials in water.

The decrease in pH in the electrocoagulation process occurs because of the alkalization process of Al_3^+ ions added in the water so that there is a reaction with a hydroxy ion from hydrolysis of water which produces Al $(OH)_3$ and hydrogen ions.

In Figure 2 we can see a decrease in pH in songket wastewater with an initial pH of 10.73 which belongs to the alkaline category, after treatment, there is a significant increase in pH which reaches pH 6.79 which is near neutral where the pH range is between 6-9.

From this graph, it can be seen that pH tends to decrease with the length of time the process with a pH range of 6-10. The best results in decreasing pH are those that occur at a current density of 45 A/ m^2 with a process time of 160 minutes which results in pH 7.39 with neutral pH.

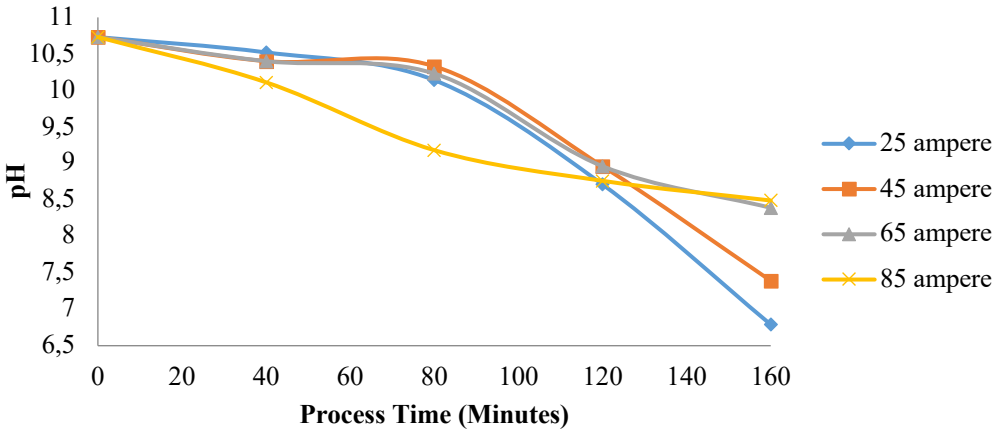

Figure 2. Graph of Effect of Current Density and Process Time on pH

Effect of Current Density and Processing Time on BOD_5

The results of electrocoagulation of songket liquid waste against the BOD5 value were seen to decrease. From Figure 3 it can be seen the best results for the decrease in BOD value is at 160 minutes and current density is 25 A/m^2 with BOD5 value 30 mg/ L, where the maximum permissible level is 50 mg/L and by electrocoagulation waste treatment with current density 25 A/m^2 and process time 160 can reduce BOD5 levels up to a value of 30 mg/L, compared with current densities and different processing times do not reach 30 mg/L, but some are below the value of 50 mg/L, and there are also which is still high above 50 mg/L which means that the current density and processing time are suitable so that it can produce a significant decrease in BOD5 levels.

The results of the BOD_5 analysis determine the quality of the body of water which is the amount of oxygen needed by microorganisms to decompose the organic matter contained in water under aerobic conditions. High BOD_5 values play an important role in determining the ability of water bodies to support the growth of algae and aquatic organisms which will result in increased growth. The higher the population of bacteria, the higher the level of water pollution.

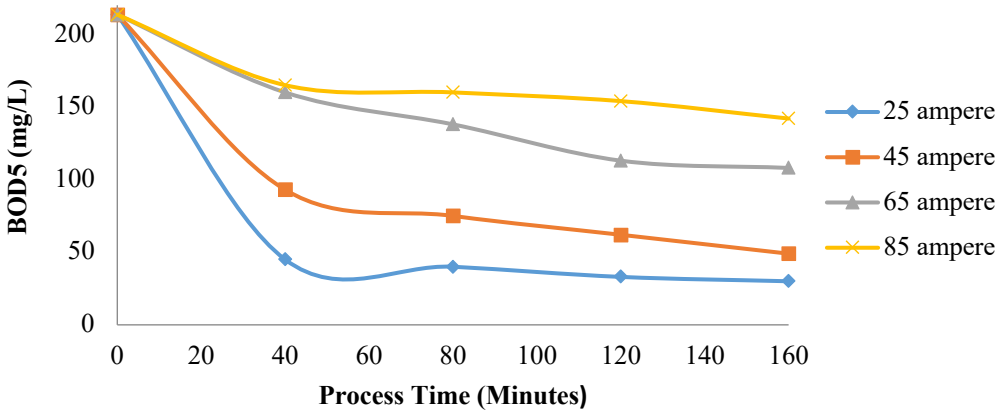

Figure 3. Graph of Effect of Current Density and Process Time on BOD_5

Effect of Current Density and Processing Time on COD

COD is the quantity or amount of oxidants that react with samples under certain conditions. The amount of oxidant used is proportional to the oxygen demand. Organic and inorganic compounds in the sample are oxidized subjects, but organic compounds are more dominant. COD is often used as a measure of the number of pollutants in water.

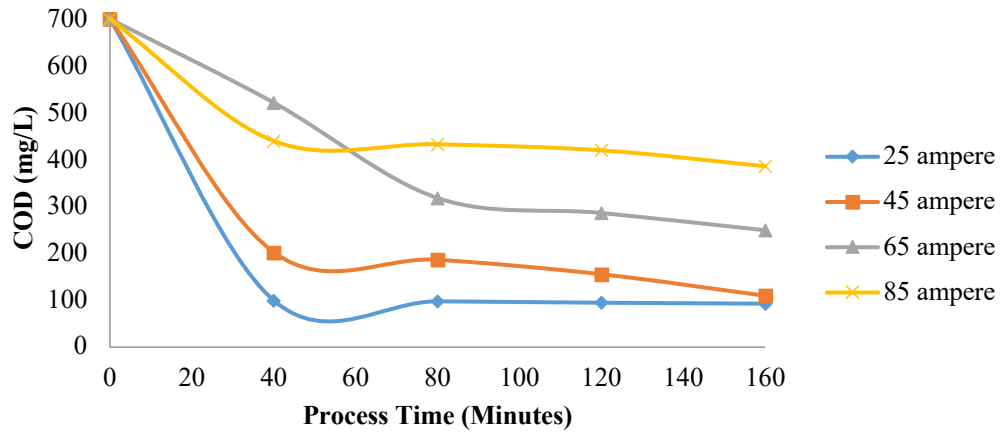

Figure 4. Graph of Effect of Current Density and Process Time on COD

Base from Figure 4, the results of the study of songket wastewater using the electrocoagulation method can be seen the best results in decreasing the value of COD at 160 minutes with a current density of 25 A/m^2 where the decrease in COD values in these conditions is very drastic from 702 mg/L to 93 mg L.

The process of decreasing the value of COD in electrocoagulation occurs through destabilization. Colloidal destruction is carried out by metal cations that form polyvalent polyhydroxide. This complex compound has a high adsorption side which makes it easier for the process of aggregation with various pollutants that form large material which is easily separated by flotation techniques because the density/density of material becomes smaller.

Effect of Current Density and Processing Time on TSS

Figure 5 shows the results of the electrocoagulation of songket liquid waste that has been carried out, the best results on a decrease in TSS value ie at 160 minutes with a current density of 25 A/m^2 where the value drops from the initial TSS value 985 mg/L to 163 mg/L, where the maximum allowed is 200 mg /L so the results at the current density of 25 A/m^2 and processing time for 160 minutes already meet the quality standard requirements. The process of decreasing TSS is very influential where TSS is a pollutant that is in a suspended form. If wastewater contains high TSS, it can be concluded that the waste is of poor quality and has the potential to damage the aquatic ecosystem in particular.

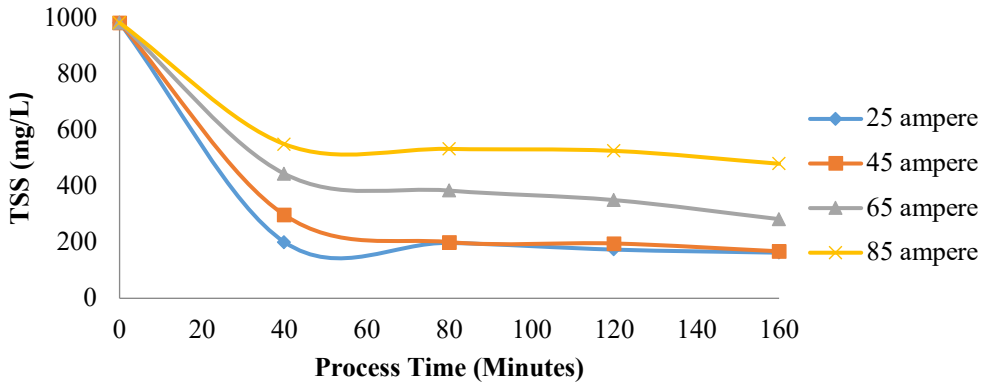

Figure 5. Graph of Effect of Current Density and Process Time on TSS

The TSS reduction process in electrocoagulation occurs when solid material from suspended solids is adsorbed into the coagulant of $Al(OH)_3$ or adsorbed into air bubbles. The results of this adsorption will be separated upwards (flexed) so that there is a decrease in TSS concentration in wastewater.

The source of TSS pollutants is both organic and inorganic chemicals that form a suspension in the wastewater. In addition, the source of TSS also comes from metals that form complex compounds both with hydroxides or other anions which these compounds are suspended in the waste solution either because of the nature of the molecular size of the compounds or the nature of the polarity possessed [12].

Effect of Current Density and Process Time on Color Intensity

From the experiments that have been done, the data shows that each change in current density and length of process time will produce different electrocoagulation efficiency. The longer the contact time, the lower the intensity of the color produced to approach the clear color. From Figure 5 it can be seen that the decrease in color intensity in the largest waste is achieved at 160 minutes process time and a current density of 25 A/m^2 from the initial results of 1120 to 24 where the water color has become clear compared to the original color of red songket liquid waste.

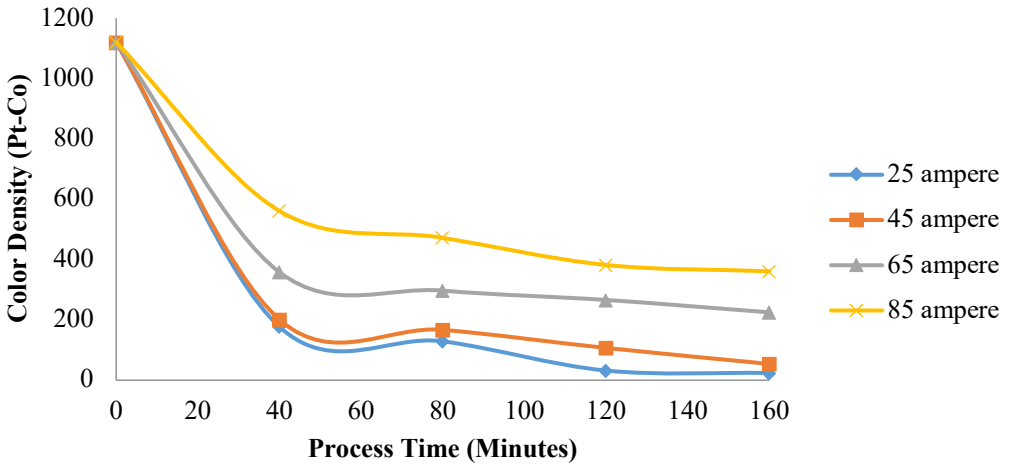

Figure 6. Graph of Effect of Current Density and Process Time on Color Intensity

Songket liquid waste contains color because in the coloring of all the dyes given will be absorbed by the thread so that it will cause the remnants of the dye. Sunlight is an important factor in photosynthesis. The results of photosynthesis will produce oxygen which will then be used to decompose organic matter.

Songket liquid waste that is colored if it is directly thrown into the water will cause color in the waters. This will inhibit the process of photosynthesis in the waters. Clean water quality standards have a color value between 5-50 PtCo [13].

Effect of Current Density and Process Time on Phenol Levels

If the water in the waters has been contaminated by phenol content, then the water is very dangerous to use. Phenol can disrupt the central nervous system which can lead to fainting and coma. Phenol can also cause hypothermia (decreased body temperature) and myocardial depression. If phenol is in contact with the skin it will cause burns, if contact with the eyes can cause irritation, swelling, corneal bleaching and ultimately blindness [14, 15]. There are many more effects of the phenol content for that phenol content in the waters is very wary and it is expected that the phenol content in the waters does not exceed the water quality standard so that it is safely used by the community.

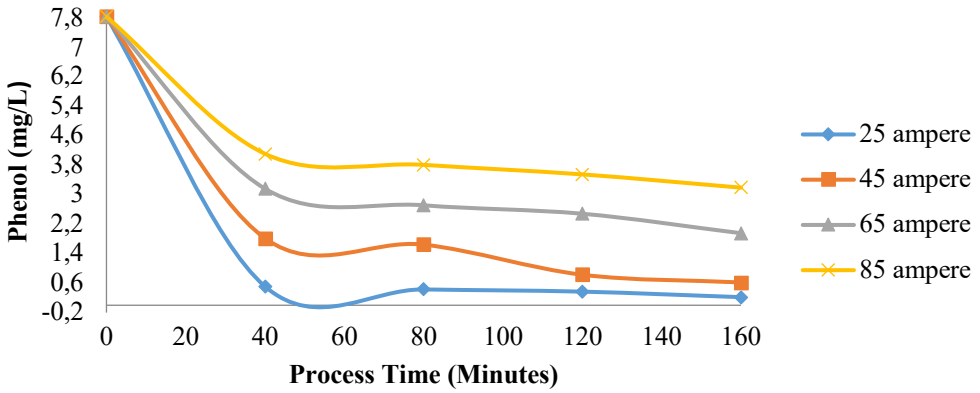

Figure 7. Graph of Effect of Current Density and Process Time on Phenol Levels

From Figure 7 it can be seen that the reduction of phenol content in the largest songket liquid waste was reached at 160 minutes at 25 A/m^2. In this condition, the phenol content in the filtrate is 0.22 mg/L from the initial analysis of 7.85 mg /L, where the maximum allowed phenol level should not be more than 0.5 mg /L.

4. CONCLUSION

Based on the results of preliminary analysis of songket liquid waste taken from songket craftsmen, the characteristics of songket liquid waste were obtained, namely pH 10.73; BOD_5 213.5 mg/L; COD 702 mg/L, TSS 985 mg/L, color intensity of 1120, and phenol content of 7.85 mg/L.

With the optimum condition of the electrocoagulation process of songket wastewater treatment for 160 minutes and current density of 25 A/m^2, the effectiveness of electrocoagulation of songket wastewater was obtained by 67.28% for TSS, 54.13% for BOD5, 63.64% for COD, 79,21% for color intensity and 74.93% for phenol levels. These results have fulfilled the textile industry wastewater quality standards.

From the research that has been done, it can be suggested that in carrying out the processing of songket industry wastewater by further electrocoagulation method to vary the voltage used and analyze the metal content in the waste.

5. REFERENCES

[1] R Rusdianasari, Y Bow, Yuniar. (2014). Treatment of Traditional Cloth Wastewater by Electrocoagulation. International Journal on Advanced Science, Engineering and Information Technology, Vol. 4, No. 2. Pp. 99-104.

[2] Depkes RI. (2010). Keputusan Menteri Kesehatan RI No. 492/Menkes/Per/IV/2010/Tentang Persyaratan Kualitas Air Minum. Jakarta.

[3] Holt, P. K., Geoffrey W. B., Mary W., and Cynthia A. M. (2002). A Quantitative Comparison Between Chemical Dosing and Electrocoagulation. Colloids and Surfaces A: Physicochem. Eng. Aspects, 211:233-248.

[4] Department of Industry and Trade and Cooperatives, Palembang. (2011). Tentang Sebaran Industri Songket di Kota Palembang Tahun 2010. Sumatera Selatan

[5] Governor. 2012. Regulations Regarding the Quality Standards of the Liquid Waste of the Textile Industry, number 08. South Sumatera.

[6] Aldilani, M. I. (2008). Penggunaan Aluminium Sebagai Sacrificial Electrode dalam Proses Elektrokoagulasi (Studi Elektrokoagulasi Larutan yang Mengandung Pewarna Tekstil). Skripsi Program Studi Kimia Jurusan Pendidikan Kimia FPMIPA UPI. Bandung: Tidak Diterbitkan.

[7] R Rusdianasari, A. Meidinariasty, I Purnamasari. (2015). Level Decreasing Kinetics Model of Heavy Metal Contents in the Coal Stockpile Wastewater with Electrocoagulation. International Journal on Advanced Science, Engineering and Information Technology, 5(6), pp. 387-391.

[8] Mollah, M. Y. A., Robert S., Jose R. P., and David L. C. (2001). Electrocoagulation (EC) – Science and Application. Journal of Hazardous Materials, B84:29-41.

[9] Mukimin, Aris. (2006). Pengolahan Limbah Industri Berbasis Logam dengan Teknologi Elektrokoagulasi Flotasi. Thesis Program Magister Ilmu Lingkungan Universitas Diponegoro, Semarang.

[10] Bazrafshan, et al., (2012). Slaughterhouse Wastewater Treatment by Combined Chemical Coagulation and Elektrocoagulation Process. PloS ONE 7(6).

[11] Y. Bow, E Sutriyono, S Nasir, and I. Hajar. (2017). Preparation of Molecularly Imprinted Polymers Simazine as Material Potentiometric Sensor. MATEC Web of Conference 101, 01002.

[12] R Rusdianasari, A Taqwa, Jaksen, A. Syakdani. (2017). Treatment Optimization of Electrocoagulation (EC) in Purifying Palm Oil Mill Effluents (POMEs). Journal of Engineering and Technology Sciences 49 (5), 604-616

[13] Maria. (2007). Studi Pendahuluan Mengenai Degradasi Zat Warna Azo (Metil Orange) dalam Pelarut Air Menggunakan Mesin Berkas Elektron 350 ke V/10 mA. JFN, Vol. 1 No. 1 Mei 2007. Yogyakarta: Sekolah Tinggi Teknologi Nuklir-Batan.

[14] Nair CI, Jayachandran K, Shashidar S. (2008). Biodegradation of Phenol. African Journal of Biotechnology 7:4951-4958.

[15] Rusdianasari, A. Taqwa. and Y. Bow. (2014). Treatment of Coal Stockpile Wastewater by Electrocoagulation using Aluminum Electrodes. Advanced Materials Research, 896, pp. 145-148.

LOGIC
Jurnal Rancang Bangun dan Teknologi
(Journal of Engineering Design and Technology)
Address : Gedung P3M, lt.1 Politeknik Negeri Bali, Bukit Jimbaran
PO BOX 1064 Kuta Selatan, Badung, Bali - Indonesia
Telp. (+62)361 701981 Fax. (+62)361 701128
Email: logic@pnb.ac.id